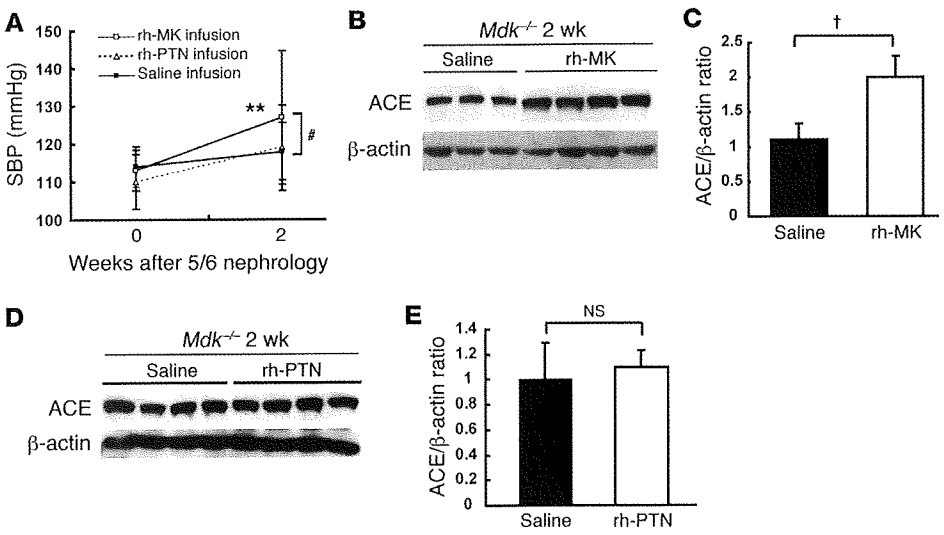

Figure 4
Effects of exogenous MK and PTN in *Mdk*$^{-/-}$ mice on blood pressure and ACE expression in the lung. (**A**) SBP was measured by the tail-cuff method at 0 and 2 weeks after 5/6 nephrectomy (n = 5). $^{**}P < 0.01$ versus untreated *Mdk*$^{-/-}$ mice (0 weeks); $^{\#}P < 0.01$, rh-MK versus saline. rh-PTN, recombinant human PTN. (**B**) ACE expression in the lung of *Mdk*$^{-/-}$ mice treated with MK and saline. Western blot data are shown. (**C**) The data in **B** were quantified using densitometry and are presented as mean and SD. $^{\dagger}P < 0.01$. (**D**) ACE expression in the lung of *Mdk*$^{-/-}$ mice treated with rh-PTN and saline. Western blot data are shown. (**E**) The data in **D** were quantified using densitometry and are presented as mean and SD.

stress induces MK expression (10, 22). Therefore, it is conceivable that Nox-mediated ROS production leads to an induction of MK expression in the lung (Figure 7). As ROS have very short half-lives (36), it is not likely that the ROS themselves travel between the kidney and lung. Furthermore, it is widely accepted that Ang II induces Nox expression (37). Based on this background data, we speculate that the following molecular circuit is established after circulating MK induces ACE expression in the lung: Ang II induces Nox expression, which in turn initiates ROS production and subsequently MK and ACE expression (Figure 7).

RAS-related inhibitors, but not hydralazine, ameliorated renal damage in the present study. It has also been reported that systemically administered Ang II worsens renal function (38–40). Therefore, the RAS might play at least a partial role in renal damage. In

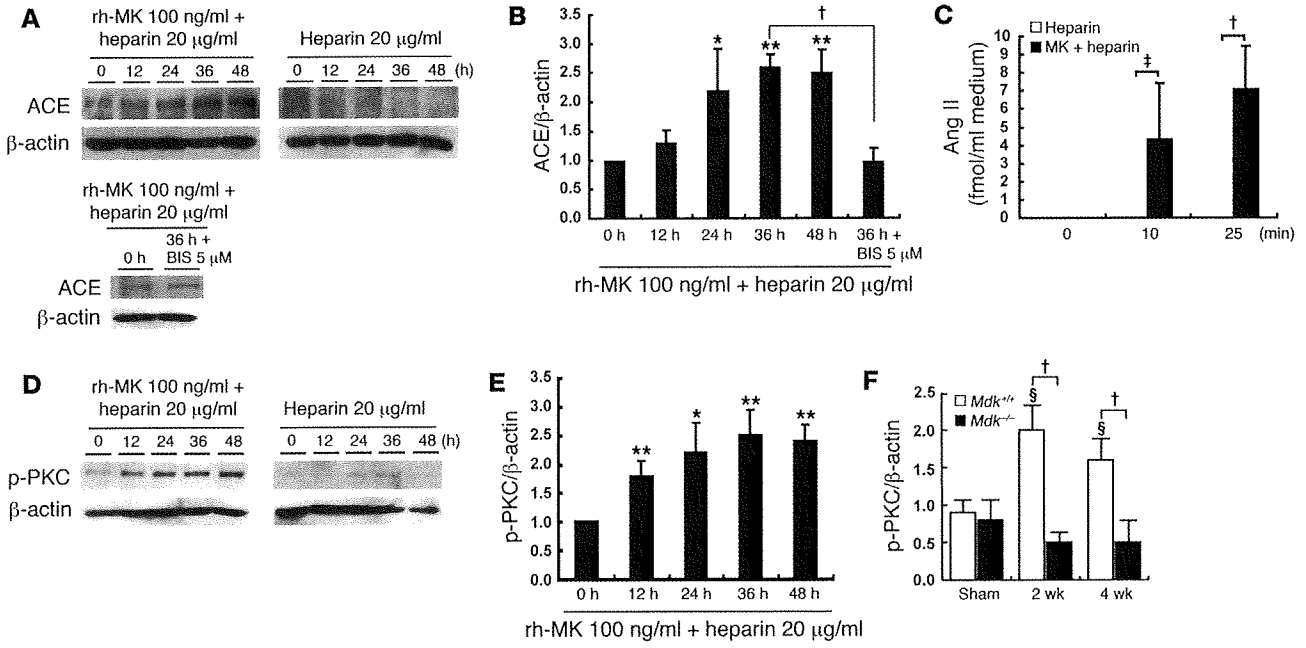

Figure 5
Mechanism of ACE induction by MK in HMVEC-L. (**A**) ACE expression in HMVEC-L treated with exogenous MK protein (100 ng/ml) and heparin (20 μg/ml). Lower panels: For PKC inhibition, BIS (5 μM) was added 1 hour before a 36-hour treatment with rh-MK plus heparin. Western blot data are shown. (**B**) The data in **A** were quantified using densitometry and are presented as mean and SD (n = 3). $^{*}P < 0.05$ and $^{**}P < 0.01$ versus 0 hours. (**C**) Conversion from Ang I to Ang II by the cells treated with MK. HMVEC-L cells were treated with exogenous MK protein (100 ng/ml) and heparin (20 μg/ml) or heparin (20 μg/ml) for 36 hours. Ang I (500 pM) was then added to the medium and incubated for the indicated times (n = 5). (**D**) Phospho-PKC expression in HMVEC-L treated with exogenous MK protein (100 ng/ml) and heparin (20 μg/ml). Western blot data are shown. (**E**) The data in **D** (left panel) were quantified using densitometry and are presented as mean and SD (n = 3). $^{*}P < 0.05$ and $^{**}P < 0.01$ versus 0 hours. (**F**) Representative data from Western blotting for phospho-PKC expression in the lung. The intensity of phospho-PKC bands on Western blotting was normalized to that of β-actin (n = 5). $^{\S}P < 0.05$ versus sham *Mdk*$^{+/+}$. Western blotting results are not shown. $^{\dagger}P < 0.01$; $^{\ddagger}P < 0.05$.

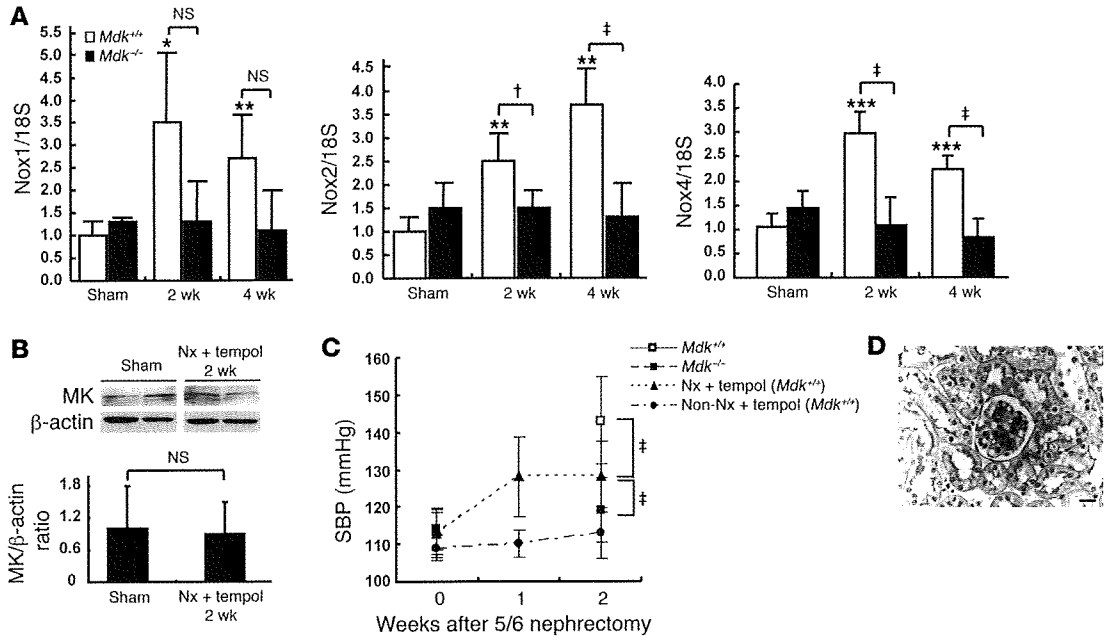

Figure 6

The mechanism of MK induction in the lung. (**A**) Time course of Nox1, -2, and -4 expression in the lung after 5/6 nephrectomy. Expression of Nox1, -2, and -4 mRNA was determined by real-time PCR. Data are presented as mean and SD ($Mdk^{+/+}$: sham, $n = 5$; 2 weeks, $n = 5$; 4 weeks, $n = 3$; $Mdk^{-/-}$: sham, $n = 3$; 2 weeks, $n = 3$; 4 weeks, $n = 3$). $^{*}P < 0.05$, $^{**}P < 0.01$, and $^{***}P < 0.001$ versus sham $Mdk^{+/+}$. (**B**) Effect of tempol on MK expression in the lung. Tempol mixed in drinking water was administered to $Mdk^{+/+}$ mice after 5/6 nephrectomy. MK protein expression was determined by Western blotting (upper panel). The intensity of MK bands on Western blotting was normalized to that of β-actin (lower panel). Data are presented as mean and SD ($n = 5$). (**C**) Effect of tempol on blood pressure after 5/6 nephrectomy. SBP was measured by the tail-cuff method. Data are presented as mean and SD ($n = 6$). (**D**) Effect of tempol on renal damage. PAS staining of a kidney specimen 2 weeks after 5/6 nephrectomy in $Mdk^{+/+}$ mice that received tempol treatment. The tubulointerstitial damage was slight compared with that in the mice without tempol treatment (Figure 1C). Scale bar: 20 μm. $^{\dagger}P < 0.05$; $^{\ddagger}P < 0.01$.

addition, we found a significant elevation of macrophage infiltration into the kidney in wild-type mice compared with $Mdk^{-/-}$ mice in the present study. This finding is consistent with our previous report showing MK-mediated macrophage recruitment in neointima formation (41). Therefore, MK-mediated inflammation in the kidney may contribute to the renal damage after 5/6 nephrectomy (Figure 7). On the other hand, in the context of inflammation and hypertension, it is important to note that inflammatory cell infiltration into the kidney does not always induce hypertension (42, 43). Furthermore, the local RAS in organs other than the lung was not activated in the present study. Thus, the relationship between intrarenal inflammation and hypertension after 5/6 nephrectomy remains to be verified.

Methods

Animals and experimental design. Mice deficient in *Mdk* were generated as described previously (44). After backcrossing of $Mdk^{+/-}$ mice for 14 generations with 129/Sv mice, $Mdk^{+/-}$ mice were mated with each other to generate $Mdk^{+/+}$ and $Mdk^{-/-}$ mice, which were used in this study. Experiments were performed on 8- to 12-week-old female mice weighing 20–25 g that were housed under controlled environmental conditions and maintained with standard food and water. Animal care and experimental procedures were approved by the Animal Experimentation Committee of the Nagoya University Graduate School of Medicine and were conducted according to the Nagoya University Regulations for Experiments. Renal ablation was performed as described previously. Briefly, mice were anesthetized by diethyl ether. The flank region was shaved, and the animals were placed on a heating pad to maintain a constant body temperature (37°C). Under anesthesia, right flank incisions were made, and the right kidney was removed. Seven days later, mice were anesthetized as above, and two-thirds of the mass of the left kidneys was ablated ($Mdk^{+/+}$: 2 weeks, $n = 13$; 4 weeks, $n = 13$; 8 weeks, $n = 8$; $Mdk^{-/-}$: 2 weeks, $n = 10$; 4 weeks, $n = 10$; 8 weeks, $n = 4$). After the renal ablation, the flanks were closed in 2 layers with 5-0 silk sutures. The animals received 100 ml/kg warm saline instilled into the peritoneal cavity during the procedure and were allowed to recover with free access to food and water. In the control mice, a sham operation was performed ($Mdk^{+/+}$, $n = 11$; $Mdk^{-/-}$, $n = 8$).

Drug treatment model. In the drug treatment studies, $Mdk^{+/+}$ mice were randomly assigned to receive one of the following 5 treatments after 5/6 nephrectomy and were orally treated daily starting from 24 hours after 5/6 nephrectomy: vasodilator (hydralazine hydrochloride; Novartis) at a dose of 10 mg/kg/d (group 1, $n = 3$); ACE inhibitor (temocapril; Daiichi Sankyo Co.) at a dose of 3 mg/kg/d (group 2, $n = 3$); angiotensin receptor blocker (olmesartan; Daiichi Sankyo Co.) at a dose of 3 mg/kg/d (group 3, $n = 3$); antioxidative reagent (tempol; Alexis Biochemicals) at a dose of 3 mmol/l in drinking solution after 5/6 nephrectomy (group 4, $n = 6$); and sham operation (group 5, $n = 6$). Drug treatment was performed at 2 weeks after 5/6 nephrectomy. In the present study, we determined the dosage according to previous reports (45–47). Blood pressure was measured by the tail-cuff method at 2 weeks, as described below under *Blood pressure monitoring*. Mice were sacrificed at 2 weeks after 5/6 nephrectomy, and blood and tissue samples were collected.

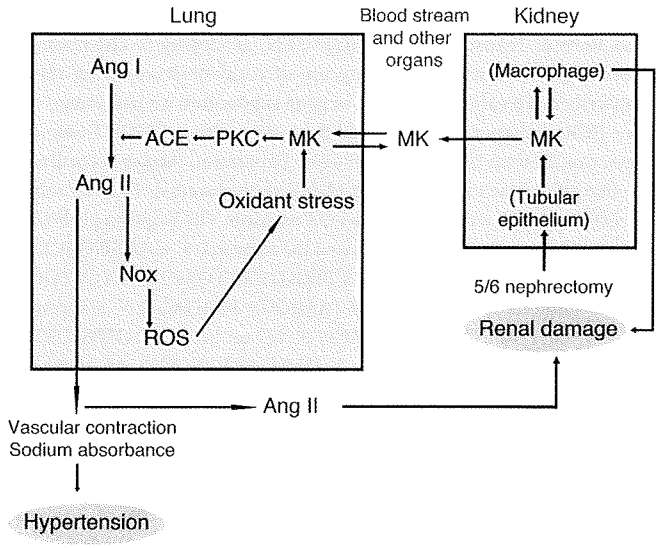

Figure 7
Schematic diagram showing the possible relationship between MK and the RAS cascade that promotes hypertension and renal damage.

MK protein and PTN protein. The recombinant human MK (rh-MK) was produced from yeast as described previously (48). In brief, human MK was produced by *Pichia pastoris* GS115 transfected with a human MK expression vector, which was constructed into pHIL-D4 (Invitrogen) (48). The MK protein was then purified by anion exchange chromatography and affinity chromatography on a heparin column. The purified human protein exhibited neurotrophic activity comparable to that of mouse MK produced in L cells (49). Recombinant human PTN was produced as previously described (50).

rh-MK and -PTN treatment model. In the pump study, MK protein in saline (1.6 mg/ml) (n = 5), PTN in saline (1.6 mg/ml; n = 5), or saline alone (n = 5) was infused using an osmotic pump (ALZA Corp.) into $Mdk^{-/-}$ mice after 5/6 nephrectomy. The pumps continuously infused a total of 100 μl over 14 days. The pumps were implanted under the dorsal skin the next day after 5/6 nephrectomy. Blood pressure was measured by the indirect tail-cuff technique at 0 and 2 weeks after 5/6 nephrectomy. Mice were sacrificed at 2 weeks after 5/6 nephrectomy, and blood and tissue samples were collected.

Blood pressure monitoring. Blood pressure was measured in restrained, conscious mice by the indirect tail-cuff technique under unstressed conditions (BP-98A; Softron) at 0, 2, 4, 6, and 8 weeks after 5/6 nephrectomy (51). Before measurement, the mice were warmed with a heating pad for 5 minutes. A total of 7–10 readings were taken for each mouse, at 1- to 2-minute intervals.

Sample collection. Mice were sacrificed at 2, 4, and 8 weeks after 5/6 nephrectomy. The remnant kidney, lung, brain, heart, and liver were removed rapidly, snap-frozen in liquid nitrogen, and stored at –80°C until examinations were performed. Each tissue was processed for histology, protein extraction, and RNA extraction. Blood samples were collected into chilled tubes for measurement of renal function parameters and into chilled tubes containing EDTA for Ang II measurements. Serum and plasma were separated by centrifugation (500 *g* for 10 minutes) and stored at –80°C until measurement were performed. Serum creatinine, blood urea nitrogen ($Mdk^{+/+}$: sham, n = 6; 2 weeks, n = 10; 4 weeks, n = 9; 8 weeks, n = 8; $Mdk^{-/-}$: sham, n = 7; 2 weeks, n = 7; 4 weeks, n = 6; 8 weeks, n = 4), and Ang II concentrations ($Mdk^{+/+}$: sham, n = 6; 2 weeks, n = 6; 4 weeks, n = 8; $Mdk^{-/-}$: sham, n = 6; 2 weeks, n = 7; 4 weeks, n = 5) were measured by Mitsubishi BCL.

ACE activity assay. Lung ACE activity was measured in a fluorescence assay using a commercial ACE activity assay kit (Life Laboratory Company, Yamagata, Japan). Isolated lung tissue ($Mdk^{+/+}$: sham, n = 5; 2 weeks, n = 5; 4 weeks, n = 5; $Mdk^{-/-}$: sham, n = 5; 2 weeks, n = 5; 4 weeks, n = 4) was homogenized in an assay buffer and then clarified by centrifugation at 10,000 *g* for 15 minutes at 4.0°C. ACE activity against a synthetic substrate (benzyloxycarbonyl-phenyl alanyl-leucine) was determined using a colorimetric method. The product was measured fluorometrically at 355-nm excitation and 460-nm emission with a fluoro-colorimeter, as follows. For the assay, tissue samples were standardized to 1 μg protein/ml. Results were calculated as mU/mg protein. All data are reported as mean ± SD. The measurements were performed in duplicate.

Histology and immunohistochemistry. The removed kidneys and lungs were fixed in 10% buffered formalin, embedded in paraffin, and then cut into 4-μm sections. The sections were stained with H&E, PAS, and Masson's trichrome. Another tissue sample was embedded in OCT compound (Sakura Finetek) and frozen in liquid nitrogen for immunostaining. Sections were cut to a thickness of 3 μm with a cryostat and fixed in acetone. High-power fields were used to examine the sections for evidence of focal sclerosis (52, 53). Glomerular sclerosis was assessed by semiquantitative score (grades 0 to +4) using the method of Raij et al. (54): grade 0, no sclerosis of glomeruli; grade 1, sclerosis of up to 25% of glomerulus; grade 2, sclerosis of 25%–50% of glomerulus; grade 3, sclerosis of 50%–75% of glomerulus; grade 4, sclerosis of 75%–100% of glomerulus. At least 50 glomeruli were evaluated under ×400 magnification and results averaged for each kidney ($Mdk^{+/+}$: 2 weeks, n = 5; 4 weeks, n = 4; 8 weeks, n = 4; $Mdk^{-/-}$: 2 weeks, n = 4; 4 weeks, n = 3; 8 weeks, n = 3). Immunostaining for ACE and MK was performed on buffered formalin-fixed tissues. Sections were deparaffinized, rehydrated, incubated in 3% hydrogen peroxide in methanol to block endogenous peroxidase, and washed in 10% normal goat serum (Dako) in PBS to block nonspecific binding. Subsequently, sections were incubated with mouse anti-ACE monoclonal antibody (dilution, 1:400; Chemicon International, Millipore) or anti-MK monoclonal antibody (dilution, 1:100) overnight at 4°C as described previously (22), followed by a conjugate of polyclonal goat anti-mouse IgG antibody and HRP-labeled polymer (Histofine Simple Stain; Nichirei) for 1 hour at room temperature as a secondary antibody. The staining was visualized with 3-3′ diaminobenzidine (Nichirei) to produce a brown color. The sections were covered with 90% glycerol containing *p*-phenylenediamine and were examined by electron microscopy (H-7100; Hitachi). For double immunofluorescence staining of MK and thrombomodulin as a marker of the vascular endothelium, the cryosections of lungs were first incubated with chicken anti-human MK (dilution, 1:200) and then with rabbit anti-rat thrombomodulin (dilution, 1:1,000) (55), followed by incubation with FITC-labeled rabbit anti-chicken IgG (dilution, 1:160) and rhodamine-labeled goat anti-rabbit IgG (dilution, 1:320) as secondary antibodies. For immunofluorescence staining of macrophages and neutrophils, the cryosections of lungs or kidneys were first incubated with rat anti-mouse F4/80 antibodies (MCA497F; dilution, 1:50; AbD Serotec) or rat anti-mouse neutrophils (MCA771G; dilution, 1:200; AbD Serotec), followed by incubation with FITC-labeled goat anti-rat IgG F(ab)′ 2 (dilution, 1:160) or FITC-labeled rabbit anti-rat IgG (dilution, 1:160) as secondary antibodies. The lung and kidney section from each mouse was viewed under ×400 magnification, and then macrophages or neutrophils were counted from 10 fields and averaged. Values are mean ± SD.

HMVEC-L culture and treatments. HMVEC-L were used for the in vitro assay because they have previously been shown to express ACE (56). HMVEC-L (Takara Bio Inc.) were cultivated in EGM-2MV BulletKit medium (Takara Bio Inc.) at 37°C in 5% CO_2. HMVEC-L were grown as a monolayer in tissue culture plates coated with type I collagen. When the cells reached 70%–80% confluence, they were passaged with trypsin (0.025%)/EDTA (0.01%) and used within 4 passages, as recommended by the supplier. After reaching

confluence, HMVEC-L were washed with PBS and cultured for 24 hours in essential basal medium containing 0.5% FBS. These cells were exposed to 100 ng/ml recombinant human MK (rh-MK) plus 20 μg/ml heparin or 50 ng/ml PMA (Sigma-Aldrich) in essential basal medium containing 0.5% FBS. PMA and the PKC inhibitor stock solutions were made in dimethyl sulfoxide. For PKC inhibition, BIS (Calbiochem) was added 1 hour before treatment with rh-MK plus heparin or PMA. Protein was extracted from HMVEC-L at the indicated time points after treatment. Cells were then lysed in RIPA buffer (50 mmol/l Tris-HCl, 150 mmol/l NaCl, 1% Nonidet P-40, 1% deoxycholic acid, and 0.05% sodium dodecyl sulfate) containing 0.25 mmol/l phenylmethylsulfonyl fluoride, kept on ice for 40 minutes, and then centrifuged at 15,000 *g* for 10 minutes at 4°C. The supernatants were then subjected to SDS-PAGE and Western blotting.

Ang II concentration in HMVEC-L. After reaching confluence, HMVEC-L were washed with PBS and cultured for 24 hours in essential basal medium containing 0.5% FBS. These cells were exposed to 100 ng/ml rh-MK plus 20 μg/ml heparin or 20 μg/ml heparin alone in essential basal medium containing 0.5% FBS for 36 hours. After stimulation, HMVEC-L were washed with PBS and exposed to 500 pM Ang I (Sigma-Aldrich) for 10 and 25 minutes. Supernatants were collected into chilled tubes, and then the Ang II concentration was measured as previously described (57).

Western blot analysis. Mouse kidney, lung, brain, heart, and liver tissues were snap-frozen in liquid nitrogen for protein isolation. Western blot analysis was performed as described previously (58). The blots were subsequently incubated with goat anti-human MK antibody (dilution, 1:1,000), monoclonal anti-β-actin antibody (dilution, 1:1,000; Sigma-Aldrich), mouse anti-ACE monoclonal antibody (dilution, 1:1,000; Chemicon International, Millipore), or rabbit anti-phospho-PKC antibody (dilution, 1:1,000; Cell Signaling Technology), followed by incubation with peroxidase-conjugated goat IgG, mouse IgG, or rabbit IgG (dilution, 1:5,000; Jackson Immunoresearch Laboratories Inc.). Western blot analysis of liver ANG was performed using the ANG-specific polyclonal antibody as described previously (59). Proteins were visualized with an enhanced chemiluminescence detection system (Amersham Pharmacia, GE Healthcare). The density of each band was measured using the public domain NIH Image program (http://rsb.info.nih.gov/nih-image/).

RNA preparation from mouse kidney and lung. Mouse kidney and lung tissues (15 mg) were immersed in RNA*later* (Ambion, Applied Biosystems) for 1 day. The mixture was ground for 2 minutes with 5-mm tungsten carbide beads at a frequency of 20–25 Hz using a mixer-mill grinder according to the manufacturer's instructions (Tissuelyser; QIAGEN). The ground solution was then centrifuged for 3 minutes at 10,000 *g* to compact the debris, and the supernatant was treated according to the manufacturer's instructions. Total RNA was extracted using an RNeasy Mini Kit (QIAGEN). RNA concentrations were estimated using a spectrophotometer (Ultrospec 3300 pro; Amersham Biosciences, GE Healthcare).

Real-time PCR. First-strand cDNA was synthesized using the QuantiTect Reverse Transcription Kit (QIAGEN) according to the manufacturer's instructions. One microgram of total RNA was then reverse transcribed. To validate changes in gene expression, we performed real-time PCR analysis with an Applied Biosystems Prism 7500HT Sequence Detection System using TaqMan Gene Expression Assays according to the manufacturer's specifications (Applied Biosystems). Two microliters of cDNA samples was used for the PCR reaction. The TaqMan probes and primers were as follows. For mouse MK: forward, 5′-CAAGGGACCCTGAAGAAGGC-3′, and reverse, 5′-CTTTGGTCTTTGACTTGCTCTTGG-3′; for ANG: forward, 5′-CTCGAACTCAAAGCAGGAGAGG-3′, and reverse, 5′-CGTAGATGGCGAACAGGAAGG-3′; for renin: 5′-TTGTTGCTCTGGAGTCCTTGC-3′, and reverse, 5′-CAGGATTTCCCGGACAGAAGG-3′; for ACE: forward, 5′-ACCCAACCTCGATGTCACCA-3′, and reverse, 5′-GCGAGGTGAAGAATTCCTCTGA-3′; for Nox1: forward, 5′-TTGGCACAGTCAGTGAGGATG-3′, and reverse, 5′-AGATTTCAAGATGGAAGCAAAGGG-3′; for Nox2: forward, 5′-ACTTTCCATAAGATGGTAGCTTGG-3′, and reverse, 5′-GCATTCACACACCACTCAACG-3′; and for Nox4: forward, 5′-ACCAGAATGAGGATCCCAGAAAG-3′, and reverse, 5′-GTAGAAGCTGTAACCATGAGGAAC-3′. 18S ribosomal RNA (assay identification number 4326317E), which was used as an endogenous control, was as assay-on-demand gene expression product (Applied Biosystems). The thermal cycler conditions were as follows: hold for 10 minutes at 95°C, followed by 2-step PCR consisting of 40 cycles at 95°C for 15 seconds and 60°C for 1 minute. The relative quantification of all targets was carried out using the comparative cycle threshold method (60). The levels of gene expression were standardized with those of the 18S ribosomal RNA.

Statistics. Results are expressed as mean ± SD. Statistical difference was assessed by a single-factor variance (ANOVA) followed by a 2-tailed unpaired *t* test, as appropriate. *P* values less than 0.05 were considered significant.

Acknowledgments

We thank Norihiko Suzuki, Naoko Asano, Yuriko Sawa, and Kayoko Miyata for their excellent technical assistance. This work was supported in part by the 21st Century COE Program and Global COE program, Ministry of Education, Culture, Sports, Science, and Technology, Japan.

Received for publication August 25, 2008, and accepted in revised form March 25, 2009.

Address correspondence to: Kenji Kadomatsu, Department of Biochemistry, Nagoya University Graduate School of Medicine, 65 Tsurumai-cho, Showa-ku, Nagoya 466-8550, Japan. Phone: 81-52-744-2059; Fax: 81-52-744-2065; E-mail: kkadoma@med.nagoya-u.ac.jp.

1. Atlas, S.A. 2007. The renin-angiotensin aldosterone system: pathophysiological role and pharmacologic inhibition. *J. Manag. Care Pharm.* **13**:9–20.
2. Kobori, H., Nangaku, M., Navar, L.G., and Nishiyama, A. 2007. The intrarenal renin-angiotensin system: from physiology to the pathobiology of hypertension and kidney disease. *Pharmacol. Rev.* **59**:251–287.
3. Ruster, C., and Wolf, G. 2006. Renin-angiotensin-aldosterone system and progression of renal disease. *J. Am. Soc. Nephrol.* **17**:2985–2991.
4. Skeggs, L.T., Jr., Kahn, J.R., Lentz, K., and Shumway, N.P. 1957. The preparation, purification, and amino acid sequence of a polypeptide renin substrate. *J. Exp. Med.* **106**:439–453.
5. Dzau, V.J. 1988. Tissue renin-angiotensin system: physiologic and pharmacologic implications. Introduction. *Circulation.* **77**:I1–I3.
6. Sayed-Tabatabaei, F.A., Oostra, B.A., Isaacs, A., van Duijn, C.M., and Witteman, J.C. 2006. ACE polymorphisms. *Circ. Res.* **98**:1123–1133.
7. Remuzzi, G., Perico, N., Macia, M., and Ruggenenti, P. 2005. The role of renin-angiotensin-aldosterone system in the progression of chronic kidney disease. *Kidney Int. Suppl.* S57–S65.
8. Kadomatsu, K., and Muramatsu, T. 2004. Midkine and pleiotrophin in neural development and cancer. *Cancer Lett.* **204**:127–143.
9. Sato, W., et al. 2005. Midkine antisense oligodeoxyribonucleotide inhibits renal damage induced by ischemic reperfusion. *Kidney Int.* **67**:1330–1339.
10. Kosugi, T., et al. 2006. Growth factor midkine is involved in the pathogenesis of diabetic nephropathy. *Am. J. Pathol.* **168**:9–19.
11. Ezquerra, L., Herradon, G., Nguyen, T., Silos-Santiago, I., and Deuel, T.F. 2005. Midkine, a newly discovered regulator of the renin-angiotensin pathway in mouse aorta: significance of the pleiotrophin/midkine developmental gene family in angiotensin II signaling. *Biochem. Biophys. Res. Commun.* **333**:636–643.
12. Werner, C., et al. 2008. RAS blockade with ARB and ACE inhibitors: current perspective on rationale and patient selection. *Clin. Res. Cardiol.* **97**:418–431.
13. Wuhl, E., and Schaefer, F. 2008. Therapeutic strategies to slow chronic kidney disease progression. *Pediatr. Nephrol.* **23**:705–716.
14. Ferrari, P. 2007. Prescribing angiotensin-converting enzyme inhibitors and angiotensin receptor blockers in chronic kidney disease. *Nephrology (Carlton).* **12**:81–89.

15. Olson, J.L., Hostetter, T.H., Rennke, H.G., Brenner, B.M., and Venkatachalam, M.A. 1982. Altered glomerular permselectivity and progressive sclerosis following extreme ablation of renal mass. *Kidney Int.* **22**:112–126.
16. Hostetter, T.H., Olson, J.L., Rennke, H.G., Venkatachalam, M.A., and Brenner, B.M. 1981. Hyperfiltration in remnant nephrons: a potentially adverse response to renal ablation. *Am. J. Physiol.* **241**:F85–F93.
17. Dikow, R., et al. 2004. Increased infarct size in uremic rats: reduced ischemia tolerance? *J. Am. Soc. Nephrol.* **15**:1530–1536.
18. van Dokkum, R.P., et al. 2004. Myocardial infarction enhances progressive renal damage in an experimental model for cardio-renal interaction. *J. Am. Soc. Nephrol.* **15**:3103–3110.
19. Pupilli, C., Chevalier, R.L., Carey, R.M., and Gomez, R.A. 1992. Distribution and content of renin and renin mRNA in remnant kidney of adult rat. *Am. J. Physiol.* **263**:F731–F738.
20. Nishimura, M., Takahashi, H., and Yoshimura, M. 2007. Upregulation of the brain renin-angiotensin system in rats with chronic renal failure. *Acta Physiol. (Oxf.).* **189**:369–377.
21. Riordan, J.F. 2003. Angiotensin-I-converting enzyme and its relatives. *Genome Biol.* **4**:225.
22. Sato, W., et al. 2001. Midkine is involved in neutrophil infiltration into the tubulointerstitium in ischemic renal injury. *J. Immunol.* **167**:3463–3469.
23. Narita, H., Chen, S., Komori, K., and Kadomatsu, K. 2008. Midkine is expressed by infiltrating macrophages in in-stent restenosis in hypercholesterolemic rabbits. *J. Vasc. Surg.* **47**:1322–1329.
24. Inoh, K., Muramatsu, H., Ochiai, K., Torii, S., and Muramatsu, T. 2004. Midkine, a heparin-binding cytokine, plays key roles in intraperitoneal adhesions. *Biochem. Biophys. Res. Commun.* **317**:108–113.
25. Villard, E., Alonso, A., Agrapart, M., Challah, M., and Soubrier, F. 1998. Induction of angiotensin I-converting enzyme transcription by a protein kinase C-dependent mechanism in human endothelial cells. *J. Biol. Chem.* **273**:25191–25197.
26. Touyz, R.M. 2003. Reactive oxygen species in vascular biology: role in arterial hypertension. *Expert Rev. Cardiovasc. Ther.* **1**:91–106.
27. Vaziri, N.D., and Rodriguez-Iturbe, B. 2006. Mechanisms of disease: oxidative stress and inflammation in the pathogenesis of hypertension. *Nat. Clin. Pract. Nephrol.* **2**:582–593.
28. Hoke, T.S., et al. 2007. Acute renal failure after bilateral nephrectomy is associated with cytokine-mediated pulmonary injury. *J. Am. Soc. Nephrol.* **18**:155–164.
29. Kelly, K.J. 2003. Distant effects of experimental renal ischemia/reperfusion injury. *J. Am. Soc. Nephrol.* **14**:1549–1558.
30. Anavekar, N.S., et al. 2004. Relation between renal dysfunction and cardiovascular outcomes after myocardial infarction. *N. Engl. J. Med.* **351**:1285–1295.
31. Amann, K., Wanner, C., and Ritz, E. 2006. Cross-talk between the kidney and the cardiovascular system. *J. Am. Soc. Nephrol.* **17**:2112–2119.
32. Kuczera, M., et al. 1991. Local angiotensin formation in hindlimbs of uremic hypertensive and renovascular hypertensive rats. *J. Hypertens.* **9**:41–48.
33. Kidney Disease Outcomes Quality Initiative (K/DOQI). 2004. K/DOQI clinical practice guidelines on hypertension and antihypertensive agents in chronic kidney disease. *Am. J. Kidney Dis.* **43**(5 Suppl. 1):S1–S290.
34. Iannone, A., Bini, A., Swartz, H.M., Tomasi, A., and Vannini, V. 1989. Metabolism in rat liver microsomes of the nitroxide spin probe tempol. *Biochem. Pharmacol.* **38**:2581–2586.
35. Schnackenberg, C.G., and Wilcox, C.S. 1999. Two-week administration of tempol attenuates both hypertension and renal excretion of 8-Iso prostaglandin f2alpha. *Hypertension.* **33**:424–428.
36. Johnson, F., and Giulivi, C. 2005. Superoxide dismutases and their impact upon human health. *Mol. Aspects Med.* **26**:340–352.
37. Mollnau, H., et al. 2002. Effects of angiotensin II infusion on the expression and function of NAD(P)H oxidase and components of nitric oxide/cGMP signaling. *Circ. Res.* **90**:E58–E65.
38. Liao, T.D., et al. 2008. Role of inflammation in the development of renal damage and dysfunction in angiotensin II-induced hypertension. *Hypertension.* **52**:256–263.
39. Kobori, H., Prieto-Carrasquero, M.C., Ozawa, Y., and Navar, L.G. 2004. AT1 receptor mediated augmentation of intrarenal angiotensinogen in angiotensin II-dependent hypertension. *Hypertension.* **43**:1126–1132.
40. Graciano, M.L., et al. 2008. Purinergic receptors contribute to early mesangial cell transformation and renal vessel hypertrophy during angiotensin II-induced hypertension. *Am. J. Physiol. Renal Physiol.* **294**:F161–F169.
41. Horiba, M., et al. 2000. Neointima formation in a restenosis model is suppressed in midkine-deficient mice. *J. Clin. Invest.* **105**:489–495.
42. Tu, X., et al. 2008. Anti-inflammatory renoprotective effect of clopidogrel and irbesartan in chronic renal injury. *J. Am. Soc. Nephrol.* **19**:77–83.
43. Usui, H.K., et al. 2007. Macrophage scavenger receptor-a-deficient mice are resistant against diabetic nephropathy through amelioration of microinflammation. *Diabetes* **56**:363–372.
44. Nakamura, E., et al. 1998. Disruption of the midkine gene (Mdk) resulted in altered expression of a calcium binding protein in the hippocampus of infant mice and their abnormal behaviour. *Genes Cells.* **3**:811–822.
45. Sada, T., Koike, H., Nishino, H., and Oizumi, K. 1989. Chronic inhibition of angiotensin converting enzyme decreases Ca2+-dependent tone of aorta in hypertensive rats. *Hypertension.* **13**:582–588.
46. Yoshida, K., Xu, H.L., Kawamura, T., Ji, L., and Kohzuki, M. 2002. Chronic angiotensin-converting enzyme inhibition and angiotensin II antagonism in rats with chronic renal failure. *J. Cardiovasc. Pharmacol.* **40**:533–542.
47. Nishiyama, A., et al. 2004. Possible contributions of reactive oxygen species and mitogen-activated protein kinase to renal injury in aldosterone/salt-induced hypertensive rats. *Hypertension.* **43**:841–848.
48. Ikematsu, S., et al. 2000. Serum midkine levels are increased in patients with various types of carcinomas. *Br. J. Cancer.* **83**:701–706.
49. Muramatsu, H., and Muramatsu, T. 1991. Purification of recombinant midkine and examination of its biological activities: functional comparison of new heparin binding factors. *Biochem. Biophys. Res. Commun.* **177**:652–658.
50. Murasugi, A., Kido, I., Kumai, H., and Asami, Y. 2003. Efficient production of recombinant human pleiotrophin in yeast, Pichia pastoris. *Biosci. Biotechnol. Biochem.* **67**:2288–2290.
51. Pfeffer, J.M., Pfeffer, M.A., and Frohlich, E.D. 1971. Validity of an indirect tail-cuff method for determining systolic arterial pressure in unanesthetized normotensive and spontaneously hypertensive rats. *J. Lab. Clin. Med.* **78**:957–962.
52. Kohzuki, M., et al. 1995. Kinin and angiotensin II receptor antagonists in rats with chronic renal failure: chronic effects on cardio- and renoprotection of angiotensin converting enzyme inhibitors. *J. Hypertens.* **13**:1785–1790.
53. Saito, T., et al. 1990. Progression of experimental focal glomerulosclerosis in the spontaneously hypertensive rat. *J. Lab. Clin. Med.* **115**:165–173.
54. Raij, L., Azar, S., and Keane, W. 1984. Mesangial immune injury, hypertension, and progressive glomerular damage in Dahl rats. *Kidney Int.* **26**:137–143.
55. Yuzawa, Y., et al. 1993. Antibody-mediated redistribution and shedding of endothelial antigens in the rabbit. *J. Immunol.* **150**:5633–5646.
56. Shen, J., Ham, R.G., and Karmiol, S. 1995. Expression of adhesion molecules in cultured human pulmonary microvascular endothelial cells. *Microvasc. Res.* **50**:360–372.
57. Nishiyama, A., Seth, D.M., and Navar, L.G. 2002. Renal interstitial fluid concentrations of angiotensins I and II in anesthetized rats. *Hypertension.* **39**:129–134.
58. Kadomatsu, K., et al. 1997. Midkine induces the transformation of NIH3T3 cells. *Br. J. Cancer.* **75**:354–359.
59. Kobori, H., Harrison-Bernard, L.M., and Navar, L.G. 2001. Expression of angiotensinogen mRNA and protein in angiotensin II-dependent hypertension. *J. Am. Soc. Nephrol.* **12**:431–439.
60. Livak, K.J., and Schmittgen, T.D. 2001. Analysis of relative gene expression data using real-time quantitative PCR and the 2(-delta delta C(T)) method. *Methods.* **25**:402–408.

Am J Physiol Renal Physiol 297: F481–F488, 2009.
First published May 20, 2009; doi:10.1152/ajprenal.00092.2009.

Effect of lowering uric acid on renal disease in the type 2 diabetic *db/db* mice

Tomoki Kosugi,[1] Takahiro Nakayama,[1] Marcelo Heinig,[1] Li Zhang,[2] Yukio Yuzawa,[3] Laura Gabriela Sanchez-Lozada,[1,4] Carlos Roncal,[1,4] Richard J. Johnson,[1,4] and Takahiko Nakagawa[1,4]

[1]*Division of Nephrology,* [2]*Molecular Pathology and Immunology Core Lab, University of Florida, Gainesville, Florida;* [3]*Department of Nephrology of Internal Medicine, Nagoya University Graduate School of Medicine, Nagoya, Japan; and* [4]*Division of Renal Disease and Hypertension, University of Colorado Denver, Aurora, Colorado*

Submitted 16 February 2009; accepted in final form 14 May 2009

Kosugi T, Nakayama T, Heinig M, Zhang L, Yuzawa Y, Sanchez-Lozada LG, Roncal C, Johnson RJ, Nakagawa T. Effect of lowering uric acid on renal disease in the type 2 diabetic *db/db* mice. *Am J Physiol Renal Physiol* 297: F481–F488, 2009. First published May 20, 2009; doi:10.1152/ajprenal.00092.2009.—Hyperuricemia has recently been recognized to be a risk factor for nephropathy in the diabetic subject. We tested the hypothesis that lowering uric acid with a xanthine oxidase inhibitor might reduce renal injury in the diabetic mouse. Diabetic (*db/db*) mice were treated with allopurinol or no treatment for 8 wk. Serum uric acid, renal function, and histology were assessed at death. The direct effect of uric acid in human proximal tubular epithelial cells was also evaluated under normal or high glucose condition. We found that *db/db* mice developed hyperuricemia, albuminuria, mesangial matrix expansion, and mild tubulointerstitial disease. Allopurinol treatment significantly lowered uric acid levels, reduced albuminuria, and ameliorated tubulointerstitial injury, but it did not prevent mesangial expansion. The mechanism for protection was shown to be due to a reduction in inflammatory cells mediated by a reduction in ICAM-1 expression by tubular epithelial cells. Interestingly, allopurinol did not reduce oxidative stress in the kidney. An inflammatory role of uric acid on tubular cells was also confirmed by our in vitro evidence that uric acid directly induced ICAM-1 expression in the human proximal tubular cell. In conclusion, hyperuricemia has a pathogenic role in the mild tubulointerstitial injury associated with diabetic nephropathy but not glomerular damage in *db/db* mice. Lowering uric acid may reduce tubulointerstitial injury in diabetes.

inflammation; monocyte chemoattractant protein-1; intercellular adhesion molecule-1

DIABETIC NEPHROPATHY IS CURRENTLY the major cause of end stage renal disease worldwide. While renin-angiotensin blockade is considered the gold standard in therapy, this treatment tends to slow renal progression rather than arrest or reverse the process. Thus we need additional therapeutic strategies to halt this epidemic.

Our group has been studying the causal role of uric acid on hypertension and renal disease (14, 19, 23). We found that experimentally induced hyperuricemia could cause hypertension and renal disease in the rat (14, 19, 23). Recently, a prospective randomized controlled trial also suggested that lowering uric acid with allopurinol could slow the progression of renal disease in patients with hyperuricemia and chronic kidney disease (31). Several epidemiological studies (2, 29, 33) have also demonstrated that serum uric acid is associated with diabetic nephropathy, suggesting a potential role for uric acid in the disease pathogenesis.

Address for reprint requests and other correspondence: T. Nakagawa, Division of Renal disease and Hypertension, Univ. of Colorado Denver, C281, Aurora, CO 80045 (e-mail: takahiko.nakagawa@ucdenver.edu).

Given these facts, we hypothesized that uric acid plays a pathological role in the development of diabetic nephropathy in type 2 diabetic *db/db* mice. To address this hypothesis, we examined the effect of lowering uric acid with allopurinol on renal histology and function in this diabetic model.

MATERIALS AND METHODS

Animals and experimental design. Diabetic *db/db* (BKS.Cg-$m^{+/+}$Lepr^{db}/J) mice and age-matched background strain C57BLKS/J mice (8 wk old, male) were purchased from the Jackson Laboratory (Bar Harbor, ME). The total of 4 groups with 10 mice per each group included *1*) control C57BLKS/J mice, *2*) control with allopurinol, *3*) *db/db* mice, and *4*) *db/db* mice with allopurinol. Allopurinol (30 mg·kg^{-1}·day^{-1}) in drinking water was administered. Systolic blood pressure was assessed using a tail cuff sphygmomanometer (Visitech BP2000; Visitech Systems, Apex, NC). Mice were killed at 8 wk after treatment. Blood samples were collected at 2, 4, and 8 wk. Urinary samples were obtained at the end of study. Blood urea nitrogen (BUN), serum uric acid levels, urinary albumin-to-creatinine ratio and uric acid were measured as described previously (24). The mean serum uric acid was calculated by using values of 2-, 6-, and 8-wk time points. All of the animal experiments were performed in accordance with the Animal Care and Use Committee of the University of Florida.

Renal histology. The removed kidneys were fixed in 10% formalin, embedded in paraffin, and then cut into 2-μm sections. The sections were used for periodic acid-Schiff (PAS) staining and immunohistochemistry. Indirect immunoperoxidase staining was performed by using antibodies to collagen IV deposition with a polyclonal rabbit anti-mouse collagen IV antibody (Chemicon International, Temecula, CA), to tubular damage with a polyclonal rabbit anti-mouse osteopontin antibody (Cosmo Bio, Tokyo, Japan), to collagen III deposition with a polyclonal goat anti-human collagen III antibody (Southern Biotechnology Associates, Birmingham, AL), and to transforming growth factor (TGF)-β expression with a rabbit polyclonal TGF-β antibody (Santa Cruz Biotechnology, Santa Cruz, CA). The staining was visualized with 3,3′-diaminobenzidine (Dako, Carpinteria, CA) for brown color development. These stained areas in cortical fields were measured by using the AxioVision image analysis computer program (Carl Zeiss, Thrornwood, NY). To assess macrophage infiltration into the tubulointerstitium, we performed immunostaining with a monoclonal anti-rat monocyte-macrophage marker F4/80 (Serotec, Oxford, UK). Macrophages positive for F4/80 were counted by examining 10 fields of the cortex under a light microscope at ×200 magnification in a blind manner. Negative controls were performed by the replacement of primary antibodies with species-matched antibodies.

Quantification of morphology. The percentage of atrophic tubules (tubular dilation, detachment of tubular epithelial cells, and condensation of tubular nuclei) was assessed by scoring 800 renal cortical tubules in randomly selected fields for each subject (17). The extent of the mesangial expansion was determined by assessing the PAS-positive and nuclei-free area in the mesangium on 40 glomeruli, as previously described (16). The glomerular area was also treated along

Table 1. *Genaral characteristics at 8 wk after treatment*

	C57BLKS/J		*db/db*	
	Control	Allopurinol	Control	Allopurinol
Body weight, g	25.2±1.5	24.6±1.2	49.1±4.2*	47.3±4.5*
Blood sugar, mg/dl	91±14	97±14	287±95*	348±112*
Blood pressure, mmHg	108±4.5	108±10	105±8.8	97±6†‡
Blood urea nitrogen, mg/dl	24±9.3	24±5.3	31±4.9	26±3.3‡
Urinary albumin-to-urinary creatinine ratio, 10^{-1}	0.28±0.18	0.21±0.14	3.7±3.0§	1.3±1.1‡

Values are means ± SE. *P < 0.0001 vs. C57BLKS/J control; †P < 0.01 vs. C57BLKS/J control; ‡P <0.05 vs. *db/db* control; §P < 0.05 vs. C57BLKS/J control.

the outline of capillary loop. Their areas were measured using the AxioVision image analysis computer program (Carl Zeiss). All quantifications were performed in a blinded manner.

Western blot analysis. Mouse kidney tissues were snap-frozen in liquid nitrogen for protein isolation. Western blot analysis was performed as described previously (18). The blots were subsequently incubated with a polyclonal goat anti-mouse ICAM-1 (R&D Systems, Minneapolis, MN), a monoclonal anti-mouse β-actin antibody (Sigma-Aldrich, St. Louis, MO), a polyclonal rabbit anti-mouse heme oxygenase (HO)-1 antibody (Stressgen, Ann Arbor, MI), or a polyclonal rabbit anti-xanthine oxidoreductase antibody (Santa Cruz Biotechnology), followed by incubation with peroxidase-conjugated goat IgG, mouse IgG, or rabbit IgG (Dako). Proteins were visualized with an ECL detection system (Amersham Pharmacia, Piscataway NJ). The density of each band was measured using the public domain National Institutes of Health Image program.

ELISA assay. ELISA assay was performed by using commercial kits for monocyte chemotactic protein (MCP-1; BD Biosciences, San Diego, CA), 8-hydroxy-2′-deoxyguanosine (OHdG; Japan Institute for the Control of Aging, Fukuroi, Shizuoka, Japan), and soluble (s)ICAM-1/CD54 (R&D Systems) according to the manufacturer's instructions.

Cell culture. Human renal proximal tubular epithelial cells (HK-2) were obtained from the American Type Culture Collection (Manassas, VA) and maintained in DMEM containing 5.4 mM D-glucose supplemented with 10% FBS. HK-2 cells were seeded on 60-mm plastic dishes. After 24 h starvation in serum-free medium, subconfluent HK-2 cells were stimulated with different concentrations (0, 7.5, or 15 mg/dl) of uric acid (Sigma-Aldrich) in the presence of 5.4 or 25 mM D-glucose (Sigma-Aldrich) for 24 or 48 h. To examine the effect of osmotic pressure of 25 mM D-glucose, 25 mM L-glucose (Sigma-Aldrich) was used as a control. The supernatants were then subjected to ELISA assay. Experiments were repeated three times.

Statistical analysis. All values are expressed as means ± SD. Statistical analysis was performed with unpaired, two-tailed Student *t*-tests for single comparisons or ANOVA with post hoc test using Tukey's method for multiple comparisons. A P value of <0.05 was taken to indicate a significant difference.

RESULTS

General characteristics. The *db/db* mice exhibited hyperglycemia and an increase in body weight during the 8 wk of the study period compared with control C57BLKS/J mice (Table 1). All mice survived. In contrast, the kidney weights in *db/db* mice were not different from those in control C57BLKS/J mice. Allopurinol treatment was well tolerated and was not associated with any difference in body weight or hyperglycemia compared with control *db/db* mice (Table 1). Allopurinol also did not alter weight or other parameters in control C57BLKS/J mice.

Uric acid levels. Serum uric acid levels tended to be higher in *db/db* mice than in control mice at 2 and 4 wk, although this was not statistically significant (Fig. 1*A*). However, mean serum uric acid for 8 wk was significantly higher in *db/db* mice compared with that in control mice, and this elevation of serum uric acid was significantly reduced by allopurinol (Fig. 1*B*). Urinary uric acid excretion (measured as the urine uric acid-to-creatinine ratio) was also increased in *db/db* mice at wk 8. The urine uric acid-to-creatinine ratio was also significantly reduced by allopurinol (Fig. 1*C*).

Renal function and blood pressure. BUN and urinary albumin excretion mice were significantly elevated in *db/db* compared with control mice, whereas systolic blood pressure was not different (Table 1). The *db/db* mice receiving allopurinol treatment had significantly lower systemic blood pressure, BUN, and albuminuria compared with untreated *db/db* mice at 8 wk. Allopurinol treatment did not affect any parameters in the control C57BLKS/J mice (Table 1).

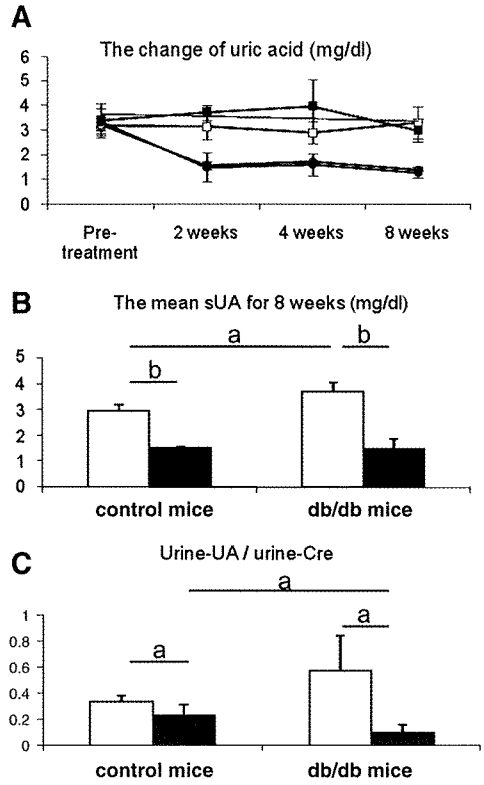

Fig. 1. Uric acid level in serum and urine in *db/db* mouse. *A*: change of serum uric acid levels. Serum uric acid tends to be high in *db/db* mouse compared with control mouse during study period (□, control mice with no treatment; ○, control with allopurinol treatment; ■, *db/db* mice with no treatment; ●, *db/db* mice with allopurinol treatment). However, the mean of serum uric acid levels for 8 wk (from 8 to 16 wk age) is significantly high in *db/db* mouse compared with control mouse. *B*: allopurinol treatment significantly reduced mean serum uric acid (sUA) level. *C*: urinary uric acid (UA) excretion is expressed the urine uric acid-to-urine creatinine (Cre) ratio. Urinary uric acid excretion is also significantly high in *db/db* mouse compared with control mouse. However, it is reduced by allopurinol treatment. □, No treatment; ■, allopurinol treatment. Data are means ± SD. [a]P < 0.05; [b]P < 0.001; n = 10/each group.

Glomerular changes. PAS staining documented glomerular mesangial expansion, an early feature of diabetic nephropathy, in *db/db* mice compared with control C57BLKS/J mice. The mesangial expansion was not prevented by allopurinol treatment in *db/db* mice (Fig. 2, *A* and *B*). Compatible with PAS staining, glomerular collagen IV deposition increased in *db/db* mice, but allopurinol had no effect on this deposition (Fig. 2, *C* and *D*).

Tubulointerstitial changes. The *db/db* mice also developed mild tubular damage as evidenced predominantly by tubular dilatation. However, allopurinol significantly reduced the tubular injury in spite of the presence of high glucose (Fig. 3, *A* and *B*). To confirm the tubulointerstitial injury and the beneficial effect of allopurinol, we examined osteopontin expression, collagen III deposition, and TGF-β expression (Fig. 3*C*). Tubular osteopontin expression was significantly induced in tubules of *db/db* mice (Fig. 3*C*, *a*), whereas this expression was reduced by allopurinol treatment (Fig. 3, *C*, *b* and *D*). Similarly, interstitial collagen III deposition (Fig. 3, *C*, *c* and *E*) and tubular TGF-β expression (Fig. 3, *C*, *e* and *F*) also increased in *db/db* mice and were blocked by allopurinol (Fig. 3, *C*, *d* and *C*, *f*, respectively). The tubular damage was significantly correlated with tubular osteopontin expression (Fig. 3*G*) and interstitial collagen III deposition (Fig. 3*H*). In contrast, nondiabetic mice with allopurinol did not show any pathological changes (Fig. 3, *D*, *E*, and *F*). Consistent with these findings, we found a positive correlation of tubular osteopontin expression with serum uric acid ($r = 0.52$; $P = 0.039$) and urine uric acid levels ($r = 0.65$; $P < 0.01$).

Inflammatory changes. We next attempted to elucidate the mechanism by which allopurinol prevented the progression of tubulointerstitial injury in *db/db* mice. Since macrophage infiltration is known to be involved in the pathogenesis of the early stage of diabetic nephropathy (8, 30) and macrophage infiltration is a hallmark of tubulointerstitial injury, we evaluated the effect of allopurinol in tubulointerstitial inflammation. As expected, macrophage infiltration was prominent in the tubulointerstitum of *db/db* mice compared with control mice. Allopurinol treatment completely blocked macrophage infiltration in *db/db* mice (Fig. 4, *A* and *B*). Compatibly, renal ICAM-1, a cell adhesion protein that is important in the inflammatory response, was also induced in *db/db* mice and was significantly reduced by allopurinol treatment (Fig. 4*D*). The *db/db* mice also exhibited an elevation in serum MCP-1 levels, which was also blocked by allopurinol treatment (Fig. 4*C*).

Oxidative stress. Since allopurinol can also block xanthine oxidase-induced oxidants, we measured oxidative stress in the kidneys of the control and allopurinol-treated mice. Xanthine

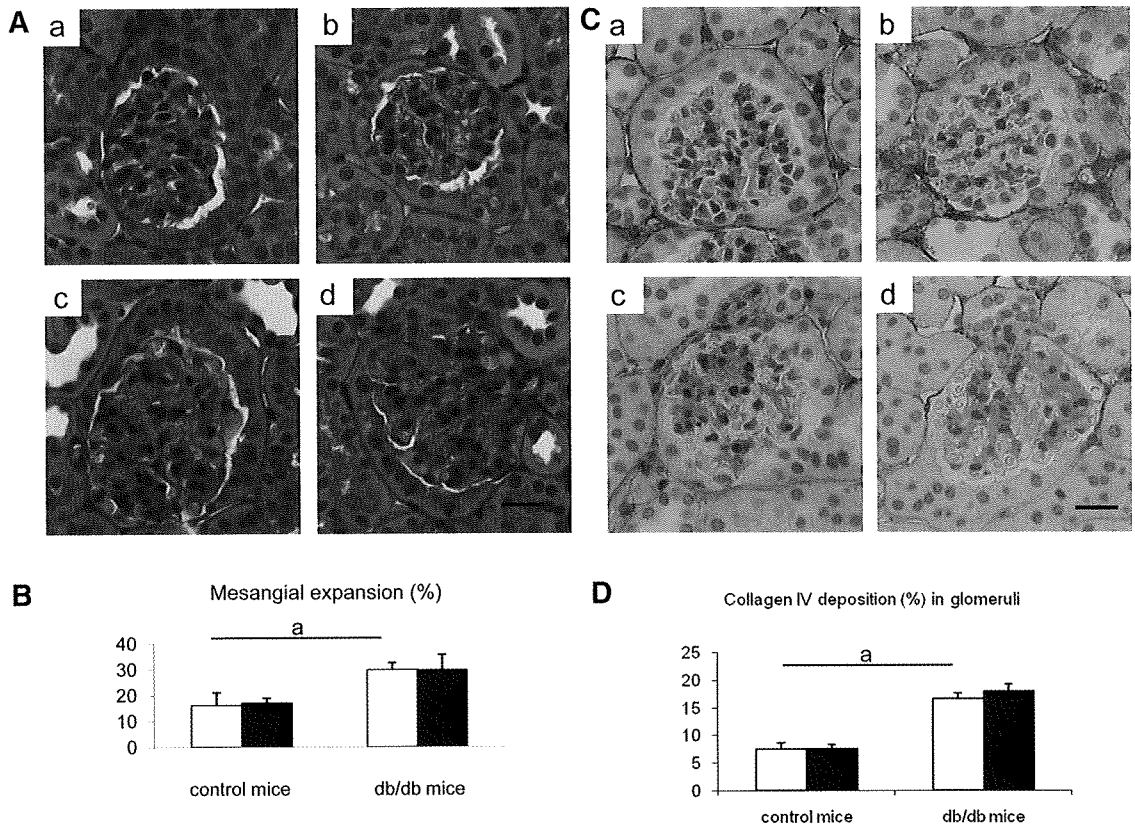

Fig. 2. Glomerular changes in *db/db* mouse. *A*: glomerular structure in periodic acid-Schiff staining. Compared with control C57BLKS/J mouse (*a*), *db/db* mouse exhibits mesangial expansion (*c*). allopurinol has no effect in glomerulus on both control (*b*) and *db/db* mouse (*d*). *B*: quantitative analysis for mesangial expansion. *C*: immunohistochemical staining shows glomerular of collagen IV depositions. Compared with glomeruli in control C57BLKS/J mouse (*a*), collagen IV deposition (brown color) increased in *db/db* mouse (*c*). Allopurinol has no effect on glomerular collagen IV deposition in both control (*b*) and *db/db* mouse (*d*). Bar = 20 μm. *D*: quantitative data for collagen IV deposition. Open bars, no treatment; filled bars, allopurinol treatment. Data are means ± SD. $^aP < 0.01$; $n = 10$/each group.

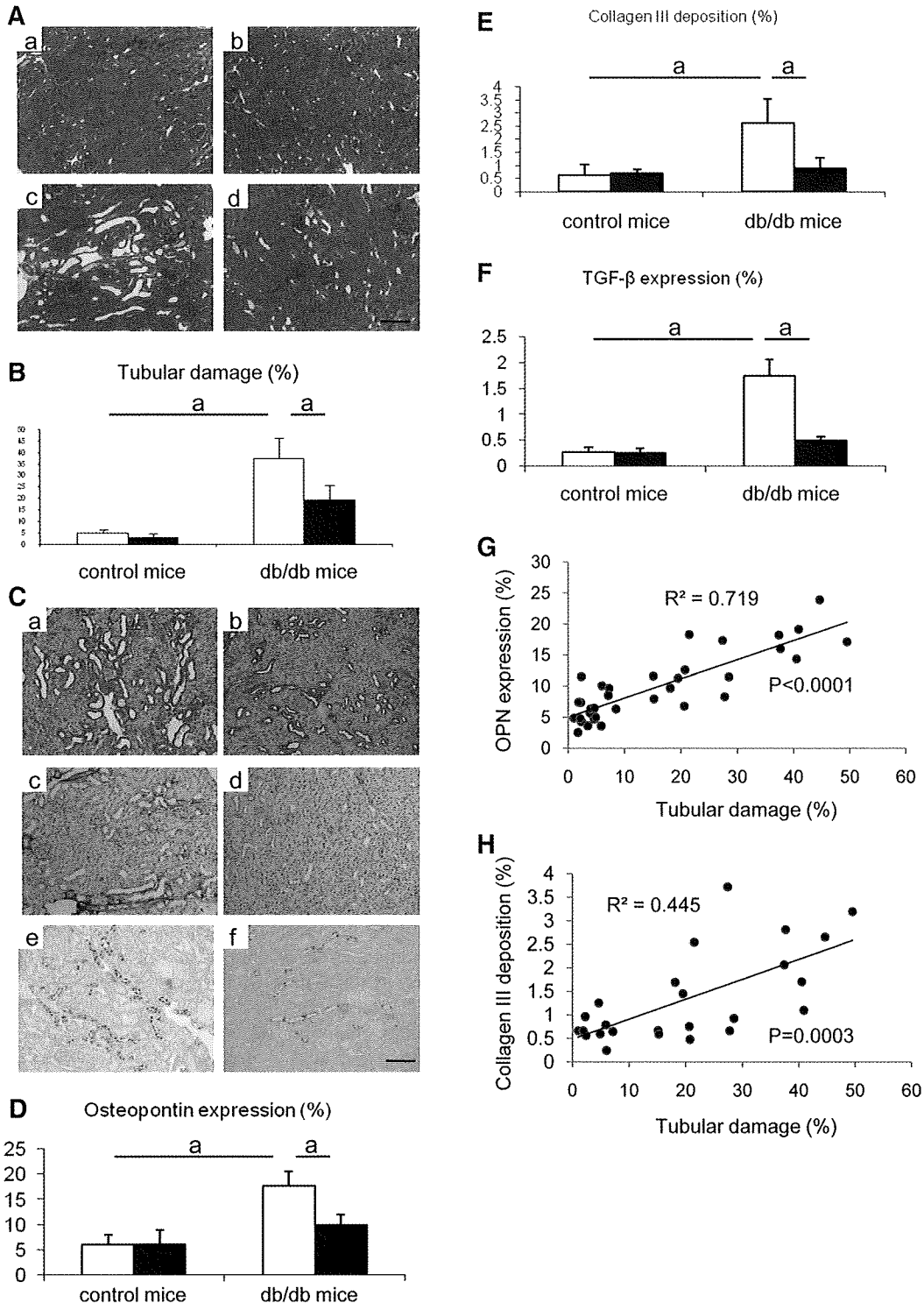

Fig. 3. Tubulointerstitial changes in *db/db* mouse. *A*: representative tubularinterstitial injuries are shown in. Compared with tubules in control mouse (*a*) and in control mouse with allopurinol treatment (*b*), *db/db* mouse (*c*) shows tubularinterstitial injury, as characterized by ballooning tubules and detachment of tubular epithelial cells from tubules. However, allopurinol treatment prevents the development of these lesions (*d*). *B*: quantitative analysis for tubulointerstitial injury. *C*: immunohistochemistry. Nontreated *db/db* mouse is shown in (*a*, *c*, *e*). *db/db* mouse with allopurinol treatment is shown in (b, d, f). Compared with nontreated *db/db* mouse, allopurinol treatment reduces osteopontin (OPN) expression (brown color) in tubules (*b*), collagen III deposition (brown color) in interstitium (*d*) and tranforming growth factor-β (TGF-β) expression (brown color) in tubules (*f*). Bar = 50 μm. Quantitative analysis is shown for OPN expression (*D*), collagen III deposition (*E*), and TGF-β expression (*F*). Also, shown is the correlation of tubular damage with OPN expression (*G*) and interstitial collagen III deposition (*H*). Open bars, no treatment; filled bars, allopurinol treatment. Data are means ± SD. $^{a}P < 0.01$; n = 10/each group.

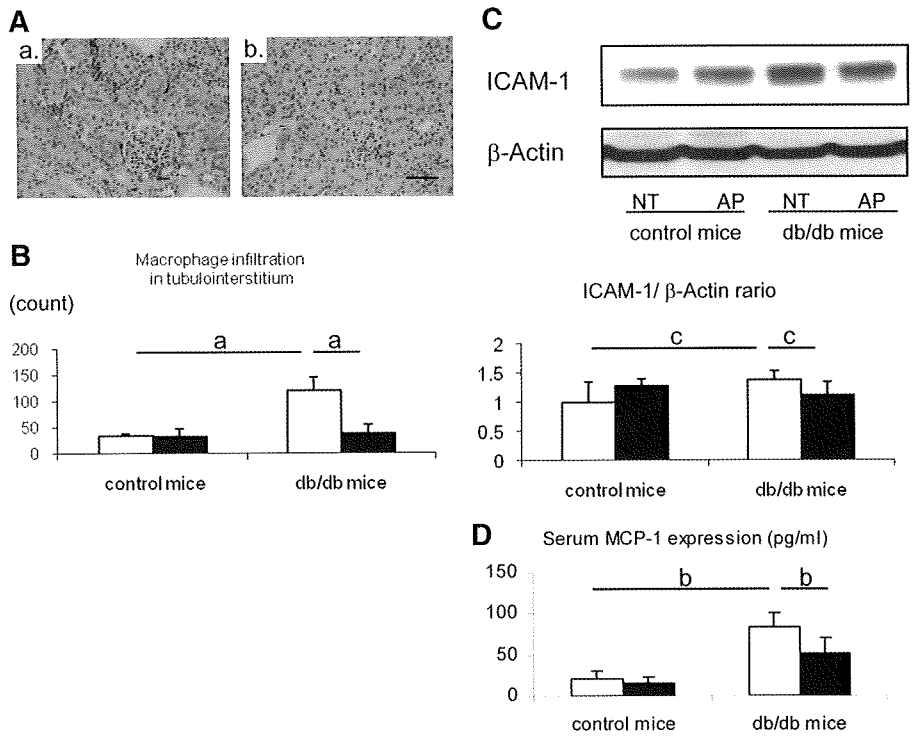

Fig. 4. Hyperuricemia-induced inflammatory response in *db/db* mouse. *A*: macrophage infiltration is examined by using immunohistochemistry for F4/80. Interstitial macrophage infiltration (brown color) is prominent in *db/db* (*a*), whereas allopurinol significantly reduces intrarenal macrophage infiltration in *db/db* mouse (*b*; bar = 50 μm). Quantitative analysis for F4/80 (+) macrophage infiltration shows that *db/db* mouse displays significantly increased macrophage infiltration in the renal cortex of *db/db* mouse. However, it is markedly prevented by allopurinol treatment (*B*). Western blotting demonstrates that ICAM-1 protein level is significantly increased in the whold kidney of *db/db* mouse, compared with control mouse. *C*: allopurinol (AP) significantly blocks the elevation of renal ICAM-1 expression compared with nontreatment mice (NT); quantitative data are expressed as the relative ratio of ICAM-1 to β-actin. *D*: ELISA assay demonstrates an elevation of serum MCP-1 levels in *db/db* mice compared with control mice and was blocked by allopurinol treatment. Open bars, no treatment; filled bars, allopurinol treatment. Data are means ± SD. $^{a}P < 0.001$; $^{b}P < 0.005$; $^{c}P < 0.05$; n = 10/each group.

oxidoreductase expression was higher in *db/db* mice compared with control mice (Fig. 5, *A* and *B*). Other markers of oxidative stress, including HO-1 and urinary 8-OHdG excretion, were also significantly higher in *db/db* mice. However, these markers of oxidative stress were not reduced by allopurinol treatment (Fig. 5, *A*, *C*, and *D*).

Induction of ICAM-1 protein on human proximal tubular epithelial cells in culture. We next determined if uric acid can directly induce inflammatory changes in cultured HK-2 cells. The expression of the ICAM-1 was measured under normal (5.4 mM D-glucose) and high glucose (25 mM D-glucose) conditions. We used 25 mM of L-glucose, which exhibits the same level of osmotic pressure as 25 mM D-glucose, as a control. At 24 h, 15 mg/dl of uric acid significantly induced sICAM-1 release under high glucose condition compared with 5 mM D-glucose, while a lower concentration (0 and 7.5 mg/dl) of uric acid did had no effect under any glucose concentrations (Fig. 6*A*), suggesting that the combination of uric acid and high glucose induced ICAM-1 expression in HK-2 cells. In contrast, at 48 h, higher concentration of uric acid significantly stimulated sICAM-1 release under normal as well as high glucose conditions (Fig. 6*B*). L-glucose tended to exhibit similar response, but it was not significant.

DISCUSSION

We found that type 2 diabetic *db/db* mice exhibit mild hyperuricemia, likely secondary due in part to increased expression of xanthine oxidoreductase within the kidney. Treatment with allopurinol lowered the serum and urinary uric acid levels, and this was associated with lower blood pressure, reduced urinary albumin excretion, improved renal function, and less tubulointerstitial injury. Interestingly, allopurinol did not improve glomerular damage. The mechanism for the renal injury might be due to the proinflammatory effects of uric acid, as renal injury was associated with increased macrophage infiltration, tubular ICAM-1 expression, and serum MCP-1 level, importantly all of which were reduced in allopurinol-treated rats. The inflammatory role of uric acid in tubular epithelial cell was also confirmed by an in vitro study in which uric acid directly induced ICAM-1 expression in human proximal tubular cells. Finally, we could not show an effect of allopurinol on urinary 8-OHdG excretion, suggesting that the beneficial effect of allopurinol might not be due to its antioxidant action. These studies suggest that treatment of diabetic nephropathy may be benefited by treatment with a xanthine oxidase inhibitor and that the mechanism may relate to preventing uric acid-induced renal inflammation.

In this study, we documented mild tubulointerstitial injury in *db/db* mice. The tubulointerstitial injury was confirmed with sensitive markers for tubular injury (osteopontin) and fibrosis (collagen III deposition). A previous study (26) of *db/db* mice also documented the presence of mild tubulointerstitial injury as evidenced by interstitial macrophage infiltration, tubular cell proliferation, and loss of peritubular capillaries, all of which were further deteriorated in nephrectomized *db/db* mice. While glomerular damage is a major feature of diabetic nephropathy, it is known that diabetic nephropathy is also associated with tubulointerstitial damage (reviewed in Refs. 10, 34), which can occasionally be a major manifestation of the disease process (6). In this case, the tubulointersisial injury was mild. While it is likely that the injury was a consequence of the diabetic state, it remains possible that other mechanisms such as leptin resistance could have a role in the injury.

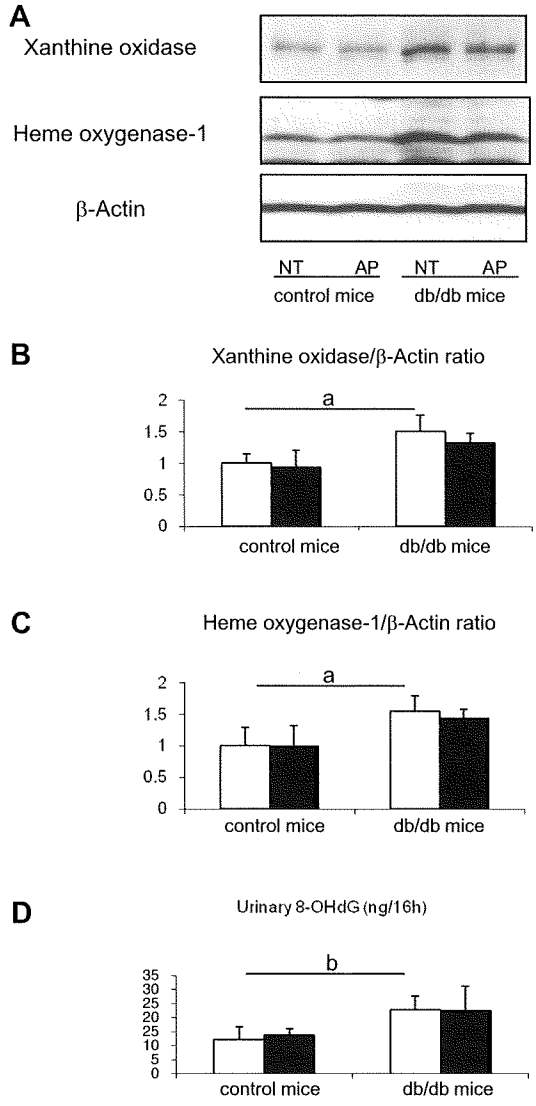

Fig. 5. Oxidative stress in *db/db* mouse. Hemoxygenase (HO)-1 and xanthine oxidase proteins in whole kidney are examined by western blotting (*A*). Quantitative results are expressed as the relative ratio of HO-1 (*B*) or xanthine oxidase (*C*) to β-actin, respectively. Both HO-1 and xanthine oxidase are significantly high in *db/db* mice compared with control mice, but these increments are not blocked by allopurinol treatment compared with nontreatment mice. ELISA assay shows that urinary 8-hydroxy-2′-deoxyguanosine (8-OHdG) levels in *db/db* mice is significantly high compared with control mice, but this induction is not inhibited by allopurinol treatment (*D*). Open bars, no treatment; filled bars, allopurinol treatment. Data are means ± SD. $^{a}P < 0.01$; $^{b}P < 0.05$; n = 10/each group.

Hypeuricemia is known to be a feature of insulin resistance syndrome (21). However, to our knowledge no investigators have yet addressed the role of hyperuricemia in diabetic nephropathy. Bo et al. (2) examined 2,113 patients with type 2 diabetes in Italy and found that hyperuricemia was associated with insulin resistance and with early onset or deterioration of diabetic nephropathy. Tseng (33) also demonstrated the association between serum uric acid and microalbuminuria in Taiwanese type 2 diabetic patients. Recently, a study (29) from the Joslin clinic documented that high normal serum uric acid was associated with a decreased renal function in type 1 diabetic patients by using serum cystain-C-based estimates glomerular filtration rates. Recently, we (11) have also collaborated with the Steno group and found that an elevated serum uric acid early in the course of type 1 diabetes can predict the development of diabetic nephropathy.

Our group has been studying the role of uric acid on hypertension and renal disease for a decade. We originally demonstrated that mild hyperuricemia causes glomerular injury and mild tubulointerstitial disease in both normal rats and rats with chronic kidney disease (14, 23). The mechanisms by which uric acid exerts renal injury involve uric acid-mediated endothelial dysfunction (15), an activation of renin angiogensin system (19), and an induction of intrarenal inflammation (13, 28). Importantly, in these hyperuricemic rats, increased macrophage infiltration is commonly observed in tubulointerstitium (14, 20, 23), suggesting a potential role of hyperuricemia on tubulointerstitial inflammation and injury.

We (28) previously reported that the potential mechanism for interstitial macrophage infiltration is attributed to the induction of intrarenal MCP-1 expression in these hyperuricemic animals. In addition, we also found that uric acid directly stimulates MCP-1 expression in vascular smooth muscle cells (13), which could account for the systemic elevation of MCP-1

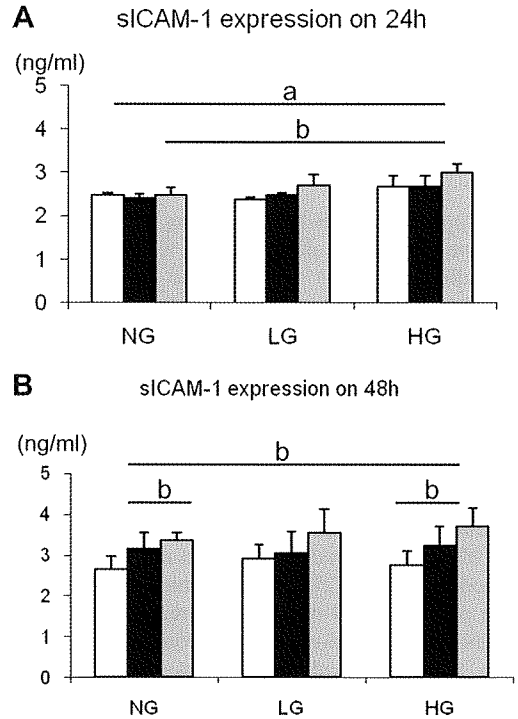

Fig. 6. Soluble intercellular adhesion molecule-1 (sICAM-1) expression in response to uric acid in HK-2 cells. HK-2 cells are stimulated by a various concentration of uric acid (0, 7.5, and 15 mg/dl) in the presence of normal D-glucose (5.4 mM; NG) or high D-glucose (HG; 25 mM) at 1 (*A*) and 2 days (*B*). L-glucose (LG) was used to examine the same level of osmotic pressure as 25 mM D-glucose loading. Open bars, 0 mg/dl uric acid; filled bars, 7.5 mg/dl uric acid; grey bars, 15 mg/dl uric acid. Data are means ± SD. $^{a}P < 0.01$; $^{b}P < 0.05$; n = 10/each group.

levels observed in this study. In addition, we newly discovered in this study that uric acid was capable of inducing ICAM-1 in tubular epithelial cell, which could contribute to the tubulointerstitial macrophage infiltration in *db/db* mice. Interestingly, our in vitro study indicated that uric acid likely induces tubular ICAM-1 expression in concert with hyperglycemia in the early time point, whereas uric acid itself turns to be potent to stimulate ICAM-1 in proximal tubular cells later. We also found that urinary excretion of uric acid was also higher in *db/db* mice. Therefore, we might need to consider the potential role of urinary uric acid in stimulating the proximal tubular cell to entry via the apical membrane.

One of the interesting findings in this study is that allopurinol improved tubulointerstitial injury but not glomerular disease in *db/db* mice. These data suggest that other factors, including high glucose or oxidative stress, could be responsible for the diabetic glomerular disease at this stage of *db/db* mice. In fact, although high glucose is well known to be one of the major stimuli to accelerate extracellular matrix deposition in diabetic glomeruli (12, 35), several studies indicated the causal role of oxidative stress in the development of diabetic glomerular injury. Suszatak et al. (32) showed that glucose-induced oxidative stress causes podocyte injury, which could initiate the development of diabetic glomerulopathy in *db/db* mice. Similarly, it was also demonstrated that the downregulation of NOX4, a subunit of NADPH oxidase, is associated with the beneficial effect of statin in experimental diabetic nephropathy (7). In this study, we confirmed that an increase in oxidative stress was associated with renal injury in *db/db* mice by using several parameters, including HO-1, xanthine oxidoreductase, and urinary OHdG. However, none of these markers was suppressed by allopurinol treatment. Thus oxidative stress may not be responsible for the tubulointerstitial injury, whereas it might contribute to the development of glomerular damage in this model.

Since allopurinol exerts both lowering uric acid and reducing oxidative stress, it is often unclear whether the beneficial effect of allopurinol can be attributed to either effect. In addition, the anti-oxidative role of allopurinol in diabetic patients is still controversial in clinical settings. Afshari et al. (1) showed that allopurinol did not reduce oxidative stress in diabetic patients, whereas another study showed a significant reduction of oxidative stress with allopurinol in type 1 diabetic patients (3). In contrast, our study is consistent with a causal role of hyperuricemia, but not oxidative stress, in the development of the tubulointerstitial injury in *db/db* mice. The failure of allopurinol to reduce oxidative stress could be due in part to its dose. While many studies used 150 mg/l of allopurinol in animal models (19, 22, 27), a recent study (9) suggests that a high dose of allopurinol may be required to reduce oxidative stress. Hence, a higher dose may be required to reduce oxidative stress, while uric acid could be lowered at lower concentration of allopurinol as demonstrated in this study.

An interesting finding was the lack of effect of allopurinol in healthy control mice. This is not dissimilar with the situation in humans in which the association of uric acid with hypertension, insulin resistance, and kidney disease occurs only when uric acid levels are greater than 5.2–5.5 mg/dl (4, 5, 25). This suggests that uric acid may require a threshold level for toxicity.

In conclusion, we demonstrated that *db/db* develop hyperuricemia, which may have a role in mediating tubulointerstitial injury associated with diabetes. Lowering uric acid improved renal function, proteinuria, and tubulointerstitial damage, and the mechanism is likely due to blocking uric acid-induced intrarenal inflammation.

GRANTS

This study was supported by the Juvenile Diabetes Research Foundation, by National Institute of Diabetes and Digestive and Kidney Diseases Grant DK-52121, by National Heart, Lung, and Blood Institute Grant HL-68607, and by generous funds from Gatorade.

DISCLOSURES

Dr. T. Nakagawa and Dr. R. J. Johnson are listed as inventors on several patent applications related to lowering uric acid as a means to reduce cardiovascular disease and diabetes.

REFERENCES

1. **Afshari M, Larijani B, Rezaie A, Mojtahedi A, Zamani MJ, Astanehi-Asghari F, Mostafalou S, Hosseinnezhad A, Heshmat R, Abdollahi M.** Ineffectiveness of allopurinol in reduction of oxidative stress in diabetic patients; a randomized, double-blind placebo-controlled clinical trial. *Biomed Pharmacother* 58: 546–550, 2004.
2. **Bo S, Cavallo-Perin P, Gentile L, Repetti E, Pagano G.** Hypouricemia and hyperuricemia in type 2 diabetes: two different phenotypes. *Eur J Clin Invest* 31: 318–321, 2001.
3. **Desco MC, Asensi M, Marquez R, Martinez-Valls J, Vento M, Pallardo FV, Sastre J, Vina J.** Xanthine oxidase is involved in free radical production in type 1 diabetes: protection by allopurinol. *Diabetes* 51: 1118–1124, 2002.
4. **Feig DI, Johnson RJ.** Hyperuricemia in childhood primary hypertension. *Hypertension* 42: 247–252, 2003.
5. **Feig DI, Kang DH, Johnson RJ.** Uric acid and cardiovascular risk. *N Engl J Med* 359: 1811–1821, 2008.
6. **Fioretto P, Mauer M, Brocco E, Velussi M, Frigato F, Muollo B, Sambataro M, Abaterusso C, Baggio B, Crepaldi G, Nosadini R.** Patterns of renal injury in NIDDM patients with microalbuminuria. *Diabetologia* 39: 1569–1576, 1996.
7. **Fujii M, Inoguchi T, Maeda Y, Sasaki S, Sawada F, Saito R, Kobayashi K, Sumimoto H, Takayanagi R.** Pitavastatin ameliorates albuminuria and renal mesangial expansion by downregulating NOX4 in db/db mice. *Kidney Int* 72: 473–480, 2007.
8. **Galkina E, Ley K.** Leukocyte recruitment and vascular injury in diabetic nephropathy. *J Am Soc Nephrol* 17: 368–377, 2006.
9. **George J, Carr E, Davies J, Belch JJ, Struthers A.** High-dose allopurinol improves endothelial function by profoundly reducing vascular oxidative stress and not by lowering uric acid. *Circulation* 114: 2508–2516, 2006.
10. **Gilbert RE, Cooper ME.** The tubulointerstitium in progressive diabetic kidney disease: more than an aftermath of glomerular injury? *Kidney Int* 56: 1627–1637, 1999.
11. **Hovind P, Possing P, Tarnow L, Johnson RJ, Parving HH.** Serum uric acid as a predictor for development of diabetic nephropathy in type 1 diabetes–an inception cohort study. *Diabetes* 2009 May 1. [Epub ahead of print].
12. **Isono M, Cruz MC, Chen S, Hong SW, Ziyadeh FN.** Extracellular signal-regulated kinase mediates stimulation of TGF-beta1 and matrix by high glucose in mesangial cells. *J Am Soc Nephrol* 11: 2222–2230, 2000.
13. **Kanellis J, Watanabe S, Li JH, Kang DH, Li P, Nakagawa T, Wamsley A, Sheikh-Hamad D, Lan HY, Feng L, Johnson RJ.** Uric acid stimulates monocyte chemoattractant protein-1 production in vascular smooth muscle cells via mitogen-activated protein kinase and cyclooxygenase-2. *Hypertension* 41: 1287–1293, 2003.
14. **Kang DH, Nakagawa T, Feng L, Watanabe S, Han L, Mazzali M, Truong L, Harris R, Johnson RJ.** A role for uric acid in the progression of renal disease. *J Am Soc Nephrol* 13: 2888–2897, 2002.
15. **Khosla UM, Zharikov S, Finch JL, Nakagawa T, Roncal C, Mu W, Krotova K, Block ER, Prabhakar S, Johnson RJ.** Hyperuricemia induces endothelial dysfunction. *Kidney Int* 67: 1739–1742, 2005.

16. **Kosugi T, Heinig M, Nakayama T, Connor T, Yuzawa Y, Li Q, Hauswirth WW, Grant MB, Croker BP, Campbell-Thompson M, Zhang L, Atkinson MA, Segal MS, Nakagawa T.** Lowering blood pressure blocks mesangiolysis and mesangial nodules, but not tubulointerstitial injury, in diabetic eNOS knockout mice. *Am J Pathol* 174: 1221–1229, 2009.
17. **Kosugi T, Yuzawa Y, Sato W, Arata-Kawai H, Suzuki N, Kato N, Matsuo S, Kadomatsu K.** Midkine is involved in tubulointerstitial inflammation associated with diabetic nephropathy. *Lab Invest* 87: 903–913, 2007.
18. **Kosugi T, Yuzawa Y, Sato W, Kawai H, Matsuo S, Takei Y, Muramatsu T, Kadomatsu K.** Growth factor midkine is involved in the pathogenesis of diabetic nephropathy. *Am J Pathol* 168: 9–19, 2006.
19. **Mazzali M, Hughes J, Kim YG, Jefferson JA, Kang DH, Gordon KL, Lan HY, Kivlighn S, Johnson RJ.** Elevated uric acid increases blood pressure in the rat by a novel crystal-independent mechanism. *Hypertension* 38: 1101–1106, 2001.
20. **Mazzali M, Kanellis J, Han L, Feng L, Xia YY, Chen Q, Kang DH, Gordon KL, Watanabe S, Nakagawa T, Lan HY, Johnson RJ.** Hyperuricemia induces a primary renal arteriolopathy in rats by a blood pressure-independent mechanism. *Am J Physiol Renal Physiol* 282: F991–F997, 2002.
21. **Modan M, Halkin H, Karasik A, Lusky A.** Elevated serum uric acid–a facet of hyperinsulinaemia. *Diabetologia* 30: 713–718, 1987.
22. **Nakagawa T, Hu H, Zharikov S, Tuttle KR, Short RA, Glushakova O, Ouyang X, Feig DI, Block ER, Herrera-Acosta J, Patel JM, Johnson RJ.** A causal role for uric acid in fructose-induced metabolic syndrome. *Am J Physiol Renal Physiol* 290: F625–F631, 2006.
23. **Nakagawa T, Mazzali M, Kang DH, Kanellis J, Watanabe S, Sanchez-Lozada LG, Rodriguez-Iturbe B, Herrera-Acosta J, Johnson RJ.** Hyperuricemia causes glomerular hypertrophy in the rat. *Am J Nephrol* 23: 2–7, 2003.
24. **Nakagawa T, Sato W, Glushakova O, Heinig M, Clarke T, Campbell-Thompson M, Yuzawa Y, Atkinson M, Johnson RJ, Croker B.** Diabetic eNOS knockout mice develop advanced diabetic nephropathy. *J Am Soc Nephrol* 18: 539–550, 2007.
25. **Nakagawa T, Tuttle KR, Short RA, Johnson RJ.** Hypothesis:fructose-induced hyperuricemia as a causal mechanism for the epidemic of the metabolic syndrome. *Nat Clinical Practice Nephorlogy* 1: 80–86, 2005.
26. **Ninichuk V, Khandoga AG, Segerer S, Loetscher P, Schlapbach A, Revesz L, Feifel R, Khandoga A, Krombach F, Nelson PJ, Schlondorff D, Anders HJ.** The role of interstitial macrophages in nephropathy of type 2 diabetic db/db mice. *Am J Pathol* 170: 1267–1276, 2007.
27. **Reungjui S, Roncal CA, Mu W, Srinivas TR, Sirivongs D, Johnson RJ, Nakagawa T.** Thiazide diuretics exacerbate fructose-induced metabolic syndrome. *J Am Soc Nephrol* 18: 2724–2731, 2007.
28. **Roncal CA, Mu W, Croker B, Reungjui S, Ouyang X, Tabah-Fisch I, Johnson RJ, Ejaz AA.** Effect of elevated serum uric acid on cisplatin-induced acute renal failure. *Am J Physiol Renal Physiol* 292: F116–F122, 2007.
29. **Rosolowsky ET, Ficociello LH, Maselli NJ, Niewczas MA, Binns AL, Roshan B, Warram JH, Krolewski AS.** High-normal serum uric acid is associated with impaired glomerular filtration rate in nonproteinuric patients with type 1 diabetes. *Clin J Am Soc Nephrol* 3: 706–713, 2008.
30. **Sato W, Kosugi T, Zhang L, Roncal CA, Heinig M, Campbell-Thompson M, Yuzawa Y, Atkinson MA, Grant MB, Croker BP, Nakagawa T.** The pivotal role of VEGF on glomerular macrophage infiltration in advanced diabetic nephropathy. *Lab Invest* 88: 949–961, 2008.
31. **Siu Y, Leung K, Tong M, Kwan T.** Use of allopurinol in slowing the progression of renal disease through its ability to lower serum uric acid level. *Am J Kidney Dis* 47: 51–59, 2006.
32. **Susztak K, Raff AC, Schiffer M, Bottinger EP.** Glucose-induced reactive oxygen species cause apoptosis of podocytes and podocyte depletion at the onset of diabetic nephropathy. *Diabetes* 55: 225–233, 2006.
33. **Tseng CH.** Correlation of uric acid and urinary albumin excretion rate in patients with type 2 diabetes mellitus in Taiwan. *Kidney Int* 68: 796–801, 2005.
34. **Ziyadeh FN.** Significance of tubulointerstitial changes in diabetic renal disease. *Kidney Int Suppl* 54: S10–S13, 1996.
35. **Ziyadeh FN, Hoffman BB, Han DC, Iglesias-De La Cruz MC, Hong SW, Isono M, Chen S, McGowan TA, Sharma K.** Long-term prevention of renal insufficiency, excess matrix gene expression, and glomerular mesangial matrix expansion by treatment with monoclonal antitransforming growth factor-beta antibody in db/db diabetic mice. *Proc Natl Acad Sci USA* 97: 8015–8020, 2000.

Biochemical and Biophysical Research Communications 380 (2009) 684–688

Contents lists available at ScienceDirect

Biochemical and Biophysical Research Communications

journal homepage: www.elsevier.com/locate/ybbrc

The hepatic circadian clock is preserved in a lipid-induced mouse model of non-alcoholic steatohepatitis

Hitoshi Ando [a,b], Toshinari Takamura [a,*], Naoto Matsuzawa-Nagata [a], Kosuke R. Shima [a], Seiji Nakamura [a], Masafumi Kumazaki [a], Seiichiro Kurita [a], Hirofumi Misu [a], Naoyuki Togawa [c], Tatsunobu Fukushima [c], Akio Fujimura [b], Shuichi Kaneko [a]

[a] Department of Disease Control and Homeostasis, Kanazawa University Graduate School of Medical Science, 13-1 Takara-machi, Kanazawa, Ishikawa 920-8641, Japan
[b] Division of Clinical Pharmacology, Department of Pharmacology, School of Medicine, Jichi Medical University, Shimotsuke, Tochigi 329-0498, Japan
[c] Yokohama Research Laboratories, Mitsubishi Rayon Co., Ltd, Yokohama, Kanagawa 230-0053, Japan

ARTICLE INFO

Article history:
Received 21 January 2009
Available online 29 January 2009

Keywords:
Atherogenic diet
Circadian rhythm
Clock gene
Non-alcoholic steatohepatitis
Oxidative stress

ABSTRACT

Recent studies have correlated metabolic diseases, such as metabolic syndrome and non-alcoholic fatty liver disease, with the circadian clock. However, whether such metabolic changes *per se* affect the circadian clock remains controversial. To address this, we investigated the daily mRNA expression profiles of clock genes in the liver of a dietary mouse model of non-alcoholic steatohepatitis (NASH) using a custom-made, high-precision DNA chip. C57BL/6J mice fed an atherogenic diet for 5 weeks developed hypercholesterolemia, oxidative stress, and NASH. DNA chip analyses revealed that the atherogenic diet had a great influence on the mRNA expression of a wide range of genes linked to mitochondrial energy production, redox regulation, and carbohydrate and lipid metabolism. However, the rhythmic mRNA expression of the clock genes in the liver remained intact. Most of the circadianly expressed genes also showed 24-h rhythmicity. These findings suggest that the biological clock is protected against such a metabolic derangement as NASH.

Various behavioral and physiological processes, including feeding behavior and energy metabolism, exhibit circadian (i.e., 24-h) rhythmicity, which may play a role in maintaining functional homeostasis. Recent studies have revealed that the circadian clock system consists essentially of a set of clock genes [1,2]. In mammals, the circadian clock resides in the hypothalamic suprachiasmatic nucleus (SCN), which is recognized as being the master clock, and in almost all peripheral tissues [3]. The SCN appears to coordinate peripheral clocks, because it is not essential for driving peripheral oscillations [3].

Rhythmic transcriptional enhancement by two basic helix–loop–helix transcription factors, CLOCK and brain and muscle Arnt-like protein 1 (BMAL1), provides the basic drive for the intracellular clock [1,2]. In parallel, the heterodimer activates the transcription of various clock-controlled genes. Given that some clock-controlled genes also serve as transcription factors, the expression of numerous genes may be tied to the functions of the circadian clock [1,2]. For example, nearly half of the known nuclear receptors, including peroxisome proliferator-activated receptors (α, γ, δ) and thyroid hormone receptors (α, β), exhibit circadian expression in liver and adipose tissues, providing a possible explanation for the cyclical behavior of carbohydrate and lipid metabolism [4].

Recent studies have demonstrated relationships between circadian clock function and the development of metabolic diseases, such as type 2 diabetes, metabolic syndrome, and non-alcoholic fatty liver disease (NAFLD). In mice, homozygous mutations in the *Clock* gene lead to the development of metabolic syndrome [5]. Moreover, we showed that the rhythmic expression of clock genes is blunted in the liver and visceral adipose tissues in KK-A^y mice, a genetic model of obese diabetes [6]. In humans, a similar effect in type 2 diabetes was found in peripheral leukocytes [7]. Furthermore, genetic variations in the *BMAL1* gene are associated with susceptibility to type 2 diabetes and hypertension [8], and *CLOCK* haplotypes are associated with metabolic syndrome [9] and NAFLD [10]. Thus, impairment of the circadian clock appears to contribute to the development of metabolic diseases.

However, whether metabolic diseases *per se* affect the circadian clock remains controversial. High glucose down-regulates mRNA expression of the clock genes (*Per1* and *Per2*) in cultured fibroblasts [11]. Additionally, the DNA-binding activity of the CLOCK-BMAL1 heterodimer is regulated by the redox state, at least *in vitro* [12]. Kohsaka et al. [13] reported that a high-fat diet affected the rhythmic mRNA expression of *Clock*, *Bmal1*, and *Per2* in the liver and adipose tissues of mice. Considering these findings, alterations in

* Corresponding author. Fax: +81 76 234 4250.
E-mail address: ttakamura@m-kanazawa.jp (T. Takamura).

0006-291X/$ - see front matter © 2009 Elsevier Inc. All rights reserved.
doi:10.1016/j.bbrc.2009.01.150

glucose, lipid, and energy metabolism; redox state; and/or the concentrations of humoral factors, such as plasma glucose, appear to influence the peripheral circadian clock. However, Oishi et al. [14] demonstrated that clock function was preserved, to a large degree, in the livers, hearts, and kidneys of mice with streptozotocin-induced insulinopenic diabetes. We also revealed that the circadian clock is hardly impaired in the liver and adipose tissues of non-obese, mild hyperglycemic Goto-Kakizaki rats [15]. Furthermore, we did not observe impairment of the circadian clock in the liver or adipose tissues of mice fed a high-fat diet, even though the mice developed metabolic syndrome, characterized by obesity, hyperlipidemia, and hyperglycemia [16]. Although the reasons for these discrepancies among the various studies are unknown, one reason might be differences in the severity of the pathological condition.

Non-alcoholic steatohepatitis (NASH) is an aggressive form of NAFLD, and the liver with steatosis and inflammation develops hepatic insulin resistance, lipotoxicity, oxidative stress, and mitochondrial abnormalities, which lead to hepatic fibrosis or cirrhosis [17]. We recently established a mouse model of NASH, induced by feeding an atherogenic diet [18]. In this model, the atherogenic diet induced steatosis, inflammation, cellular ballooning, stellate cell activation, hepatic insulin resistance, lipid peroxidation, and oxidative stress in the liver; it finally caused hepatic cirrhosis. Thus, the pathological conditions in the liver of this model are complex and quite severe compared with those of mice fed a simple high-fat diet [13,16]. Therefore, it is reasonable to expect that the hepatic circadian clock may be impaired in this model, if the alterations in metabolism and redox state affect the oscillator. To test this, we developed a custom-made, high-precision DNA chip useful for analyzing the metabolic status of the liver and investigated the rhythmic mRNA expression of clock genes and genes linked to carbohydrate and lipid metabolism, energy production, and redox regulation in the livers of mice fed an atherogenic diet.

Materials and methods

Mice. Male C57BL/6J mice (Charles River Laboratories Japan, Yokohama, Japan) were obtained at 5 weeks of age and maintained under conditions of controlled temperature and humidity and a 12-h light (08:45–20:45 h)/12-h dark (20:45–08:45 h) cycle. Mice had free access to food and drinking water. After 3 days of acclimation, the mice were divided into two groups. Half of the mice ($n = 16$) were fed a standard laboratory diet (CRF-1, Oriental Yeast Co., Tokyo, Japan), whereas the others ($n = 16$) were given an atherogenic diet (Research Diets, New Brunswick, NJ) containing 34.3% fat (lard, soybean oil), 25.8% protein (casein, L-cystine), 24.6% carbohydrate (maltodextrin, sucrose), 1.3% cholesterol, 0.5% sodium cholate, 5.7% mineral mixture, 1.5% vitamin mixture, and 6.3% cellulose. After 5 weeks of feeding, animals were sacrificed to obtain blood and liver samples at the following zeitgeber times (ZT): 0, 6, 12, and 18, in which ZT 0 is defined as lights on and ZT 12 as lights off.

All animal procedures were performed in accordance with the standards set forth in the Guidelines for the Care and Use of Laboratory Animals at the Takara-machi campus of Kanazawa University (Kanazawa, Japan).

Statistical analyses. Differences in the variables and mRNA levels between mice fed the atherogenic diet and control mice were evaluated using Student's t test. The rhythmicity of each gene was assessed using one-way ANOVA. The values are presented as the means ± SEM, and $P < 0.05$ was deemed to indicate statistical significance. All calculations were performed using SPSS software (version 11 for Windows, SPSS Japan, Tokyo, Japan).

Additional details on methods. For details on the blood chemistry, DNA chip analysis, and real-time quantitative PCR, see Supplemental Materials and methods.

Results

Development of a custom-made DNA chip suitable for metabolic research

We established a database of hepatic gene expression profiles in various human diseases, and rodent models of diabetes and/or obesity. The models include patients with type 2 diabetes, with or without obesity [19–24] and NAFLD [25]; genetic rodent models of type 2 diabetes and/or obesity [6,26]; diet-induced rodent models of obesity [27]; diet-induced rodent models of NAFLD [18,28,29]; and a rodent model of ischemic heart disease (manuscript submitted). We extracted the significantly altered genes in each metabolic pathway both in human diseases and animal models and selected 190 mouse genes linked to the circadian clock, energy production, redox regulation, ROS defense, MAPK cascade, energy and cholesterol metabolism, and protein degradation. Because expression of 70 of these genes was hardly detected in a liver sample (FirstChoice mouse liver total RNA, Applied Biosystems) or was determined differently from the results analyzed by real-time PCR, we used data for the other 120 genes for analyses in this study (Supplemental Table 1). The results of the 120 genes analyzed by the DNA chip strongly correlated with those obtained by real-time PCR (Pearson's correlation coefficient $r = 0.963$, $P < 0.0001$; Supplemental Fig. 2).

Mouse model of NASH induced by feeding an atherogenic diet

As reported previously [18], mice fed an atherogenic diet for 5 weeks developed NASH, diagnosed based on histology (Supplemental Fig. 3). Serum concentrations of ALT and total cholesterol in mice fed the atherogenic diet were significantly higher than those in control mice (Table 1). The concentration of d-ROMs was also elevated, suggesting that oxidative stress was induced in the mice on the atherogenic diet.

Global gene expression profile in the livers of mice fed an atherogenic diet

Consistent with the histological and biochemical findings, the DNA chip analyses revealed that the atherogenic diet had a wide influence on mRNA expression, affecting genes linked to energy production, redox regulation, ROS defense, the MAPK cascade, nuclear receptors, energy and cholesterol metabolism, and protein degradation (Supplemental Table 2). In most of the genes examined, the atherogenic diet decreased transcript levels. Specifically,

Table 1
Metabolic parameters in mice fed a regular or atherogenic diet.

Parameter	Control	Atherogenic	P
Body weight (g)	28.7 ± 0.8	23.2 ± 0.9	<0.01
Blood glucose (mg/dL)	166 ± 5	163 ± 8	0.73
Serum ALT (U/L)	18 ± 1	51 ± 7	<0.01
Serum total cholesterol (mg/dL)	98 ± 2	151 ± 7	<0.01
Serum HDL-cholesterol (mg/dL)	71 ± 2	71 ± 3	0.90
Serum triglyceride (mg/dL)	80 ± 13	14 ± 2	<0.01
d-ROMs (U)	20 ± 1	34 ± 3	<0.01

Blood samples were obtained from non-fasted mice at zeightgeber time 0 and 12 ($n = 4$ for each time point in both groups).
Data are means ± SEM of eight mice.
ALT, alanine aminotransferase; HDL, high-density lipoprotein; d-ROMs, derivatives of reactive oxygen metabolites.

the mRNA expression for 35 of 47 genes linked to energy production and redox regulation, 11 of 16 energy metabolism-related genes, and five of six cholesterol metabolism-related genes was significantly suppressed at one or more time points. However, there was no significant difference in the hepatic mRNA expression levels of clock genes between the mice fed the atherogenic diet and control mice at any time point (Supplemental Table 2). This finding was verified by real-time quantitative PCR (Fig. 1).

In control mice, the DNA chip analyses detected rhythmic mRNA expression in 31 genes, in addition to the clock genes (Fig. 2, Supplemental Fig. 4 and Supplemental Table 1). As reported previously [16], daily expression profiles of *Cyp7a1* gene were opposite in phase between the groups (Fig. 2D). Additionally, the atherogenic diet dampened the mRNA expression rhythms in two of two genes related to ROS defense and seven of eight genes involved in protein degradation (Fig. 2E, Supplemental Fig. 4A and Supplemental Table 1). However, transcript levels of most of the genes related to energy production, redox regulation, MAPK cascade, nuclear receptors, and energy and cholesterol metabolism, as well as the clock genes, showed significant 24-h rhythmicity in mice fed the atherogenic diet and in control mice (Fig. 2A–D, Supplemental Fig. 4B and Supplemental Table 1). These results suggest that the circadian clock function is maintained in the livers of mice with NASH, probably due to compensating alterations in the expression of various genes, including ROS defense- and protein degradation-associated genes.

Discussion

Accumulating evidence shows that the circadian clock regulates many physiological functions, such as carbohydrate and lipid metabolism [4], mitochondrial energy production, redox regulation, ROS defense [30,31], and MAPK activity [32]. Thus, it is not surprising that dysfunction in the circadian clock can cause various disorders, including metabolic syndrome [5] and malignancies [33]. However, whether these pathological conditions *per se* cause impairment of clock function remains to be clarified. In particular, our previous finding [16] that simple fatty liver induced by high-fat feeding had little effect on the hepatic circadian clock in mice differs considerably from the results of Kohsaka et al. [13]. To address this issue, we developed a severe NASH model, with oxidative stress and drastic metabolic changes, and investigated the expression rhythms of the clock genes and metabolism- and inflammation-associated genes in the liver of this animal model.

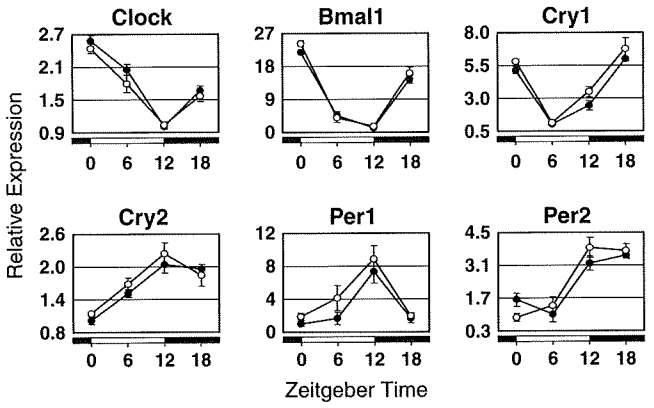

Fig. 1. Daily mRNA expression profiles of clock genes in the livers of mice fed a regular (black circles) or an atherogenic (white circles) diet. Transcript levels of the clock genes were determined by real-time quantitative PCR. Data are means ± SEM of four mice at each time point and are expressed as relative values to the lowest values in control mice for each gene.

As expected, the atherogenic diet altered the mRNA expression of various genes related to energy production, redox regulation, the MAPK cascade, and carbohydrate and lipid metabolism. Additionally, these effects on mRNA expression exhibited daily variation; they became marked during the dark/active phase. Because the light condition and daily feeding profile did not differ between mice fed the atherogenic diet and control mice, the daily variation in the intake of the atherogenic diet components may have caused the difference between mRNA expression profiles in the dark and light phases. However, the intracellular clock remained intact under these drastically altered conditions. These results suggest that the circadian clock is protected against, or not susceptible to, alterations in the intracellular environment, including redox state and metabolism.

Light and dietary intake strongly entrain the master and hepatic clocks, respectively [2,31]. The master clock in the SCN may synchronize the peripheral oscillators, at least partly via the autonomic nervous system [2]. In this study, the mice with NASH were maintained on a well-regulated 12-h light/12-h dark cycle. Additionally, their daily feeding rhythm did not differ from that of control mice (data not shown). Under this condition, the hepatic clock ticked normally. Kohsaka et al. [13] reported that a high-fat diet lengthened the period of locomotor activity rhythm under constant darkness in mice, but the effect was not detected under a 12-h light/12-h dark cycle. Moreover, night-time restricted feeding can normalize the impaired circadian clock in the livers of db/db mice [34]. These results suggest that the signals induced by light and feeding can entrain the hepatic circadian clock, even in the face of the alterations of metabolism and redox state. The influence of a high-fat diet on the hepatic clock may have been observed by Kohsaka et al. [13], but not us [16], due to differences in daily feeding rhythm, which was dampened in their study but not in ours.

Consistent with the intact intracellular clock, the daily expression rhythms of most circadianly expressed genes examined were preserved in the livers of mice with NASH. However, the 24-h expression rhythms of some genes were blunted or changed by the atherogenic diet. It is interesting that the expression rhythms of genes involved in protein degradation were markedly changed in the mice with NASH. The clock proteins, as well as the other short-lived proteins, are degraded by the ubiquitin-proteasome system [2]. Degradation rates of the clock proteins are controlled by their phosphorylation [2] and binding to an F-box protein [35]. These post-translational regulation mechanisms may account for the fact that Cry2 protein accumulates with a markedly higher circadian amplitude than *Cry2* mRNA [36]. Further studies are needed to determine whether the degradation rates of clock proteins are altered to compensate for the effects of the atherogenic diet.

In conclusion, the atherogenic diet caused NASH and alterations in the intracellular environment, affecting energy metabolism, protein degradation, and redox state. However, these conditions did not impair the circadian clock or the expression rhythms of most of the genes examined in the liver. These findings provide evidence that the circadian clock is protected against alterations in the intracellular environment, including metabolism and redox state. The impairment of biological clock appears to be important as a cause of metabolic disease.

Acknowledgments

This work was supported by in part of a Grant-in-Aid for Scientific Research from the Ministry of Education, Culture, Sports, Science and Technology, Japan.

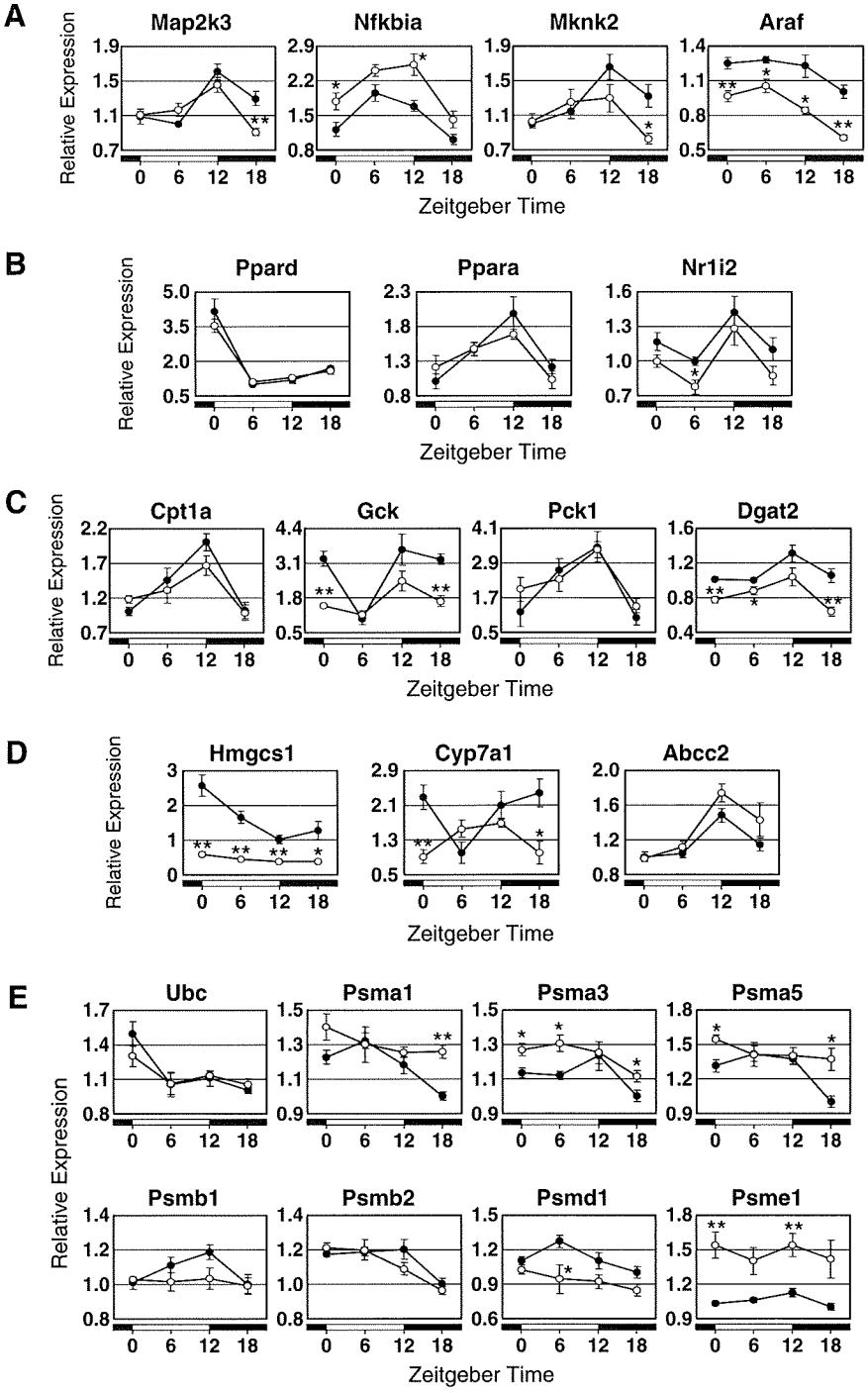

Fig. 2. Daily mRNA expression profiles of the circadianly expressed genes related to the MAPK cascade (A), nuclear receptors (B), energy metabolism (C), cholesterol metabolism (D), and protein degradation (E) in the livers of mice fed a regular (black circles) or an atherogenic (white circles) diet. Transcript levels of the clock genes were determined by the custom-made, high-precision DNA chip. Data are means ± SEM of four mice at each time point and are expressed as relative values to the lowest value in control mice for each gene. $^{*}P < 0.05$, $^{**}P < 0.01$, *vs.* control mice.

Appendix A. Supplementary data

Supplementary data associated with this article can be found, in the online version, at doi:10.1016/j.bbrc.2009.01.150.

References

[1] P.L. Lowrey, J.S. Takahashi, Mammalian circadian biology: elucidating genome-wide levels of temporal organization, Annu. Rev. Genomics Hum. Genet. 5 (2004) 407–441.

[2] S.M. Reppert, D.R. Weaver, Coordination of circadian timing in mammals, Nature 418 (2002) 935–941.

[3] S.H. Yoo, S. Yamazaki, P.L. Lowrey, K. Shimomura, C.H. Ko, E.D. Buhr, S.M. Siepka, H.K. Hong, W.J. Oh, O.J. Yoo, M. Menaker, J.S. Takahashi, PERIOD2::LUCIFERASE real-time reporting of circadian dynamics reveals persistent circadian oscillations in mouse peripheral tissues, Proc. Natl. Acad. Sci. USA 101 (2004) 5339–5346.

[4] X. Yang, M. Downes, R.T. Yu, A.L. Bookout, W. He, M. Straume, D.J. Mangelsdorf, R.M. Evans, Nuclear receptor expression links the circadian clock to metabolism, Cell 126 (2006) 801–810.

[5] F.W. Turek, C. Joshu, A. Kohsaka, E. Lin, G. Ivanova, E. McDearmon, A. Laposky, S. Losee-Olson, A. Easton, D.R. Jensen, R.H. Eckel, J.S. Takahashi, J. Bass, Obesity

and metabolic syndrome in circadian Clock mutant mice, Science 308 (2005) 1043–1045.
[6] H. Ando, H. Yanagihara, Y. Hayashi, Y. Obi, S. Tsuruoka, T. Takamura, S. Kaneko, A. Fujimura, Rhythmic messenger ribonucleic acid expression of clock genes and adipocytokines in mouse visceral adipose tissue, Endocrinology 146 (2005) 5631–5636.
[7] H. Ando, T. Takamura, N. Matsuzawa-Nagata, K.R. Shima, T. Eto, H. Misu, M. Shiramoto, T. Tsuru, S. Irie, A. Fujimura, S. Kaneko, Clock gene expression in peripheral leucocytes of patients with type 2 diabetes, Diabetologia 52 (2009) 329–335.
[8] P.Y. Woon, P.J. Kaisaki, J. Braganca, M.T. Bihoreau, J.C. Levy, M. Farrall, D. Gauguier, Aryl hydrocarbon receptor nuclear translocator-like (BMAL1) is associated with susceptibility to hypertension and type 2 diabetes, Proc. Natl. Acad. Sci. USA 104 (2007) 14412–14417.
[9] E.M. Scott, A.M. Carter, P.J. Grant, Association between polymorphisms in the Clock geneobesity and the metabolic syndrome in man, Int. J. Obes. (Lond.) 32 (2008) 658–662.
[10] S. Sookoian, G. Castano, C. Gemma, T.F. Gianotti, C.J. Pirola, Common genetic variations in CLOCK transcription factor are associated with nonalcoholic fatty liver disease, World J. Gastroenterol. 13 (2007) 4242–4248.
[11] T. Hirota, T. Okano, K. Kokame, H. Shirotani-Ikejima, T. Miyata, Y. Fukada, Glucose down-regulates Per1 and Per2 mRNA levels and induces circadian gene expression in cultured Rat-1 fibroblasts, J. Biol. Chem. 277 (2002) 44244–44251.
[12] J. Rutter, M. Reick, L.C. Wu, S.L. McKnight, Regulation of clock and NPAS2 DNA binding by the redox state of NAD cofactors, Science 293 (2001) 510–514.
[13] A. Kohsaka, A.D. Laposky, K.M. Ramsey, C. Estrada, C. Joshu, Y. Kobayashi, F.W. Turek, J. Bass, High-fat diet disrupts behavioral and molecular circadian rhythms in mice, Cell Metab. 6 (2007) 414–421.
[14] K. Oishi, M. Kasamatsu, N. Ishida, Gene- and tissue-specific alterations of circadian clock gene expression in streptozotocin-induced diabetic mice under restricted feeding, Biochem. Biophys. Res. Commun. 317 (2004) 330–334.
[15] H. Ando, K. Ushijima, H. Yanagihara, Y. Hayashi, T. Takamura, S. Kaneko, A. Fujimura, Clock gene expression in the liver and adipose tissues of non-obese type 2 diabetic Goto-Kakizaki rats, Clin. Exp. Hypertens., in press.
[16] H. Yanagihara, H. Ando, Y. Hayashi, Y. Obi, A. Fujimura, High-fat feeding exerts minimal effects on rhythmic mRNA expression of clock genes in mouse peripheral tissues, Chronobiol. Int. 23 (2006) 905–914.
[17] G.C. Farrell, C.Z. Larter, Nonalcoholic fatty liver disease: from steatosis to cirrhosis, Hepatology 43 (2006) S99–S112.
[18] N. Matsuzawa, T. Takamura, S. Kurita, H. Misu, T. Ota, H. Ando, M. Yokoyama, M. Honda, Y. Zen, Y. Nakanuma, K. Miyamoto, S. Kaneko, Lipid-induced oxidative stress causes steatohepatitis in mice fed an atherogenic diet, Hepatology 46 (2007) 1392–1403.
[19] T. Takamura, M. Sakurai, T. Ota, H. Ando, M. Honda, S. Kaneko, Genes for systemic vascular complications are differentially expressed in the livers of type 2 diabetic patients, Diabetologia 47 (2004) 638–647.
[20] Y. Takeshita, T. Takamura, E. Hamaguchi, A. Shimizu, T. Ota, M. Sakurai, S. Kaneko, Tumor necrosis factor-alpha-induced production of plasminogen activator inhibitor 1 and its regulation by pioglitazone and cerivastatin in a nonmalignant human hepatocyte cell line, Metabolism 55 (2006) 1464–1472.
[21] H. Misu, T. Takamura, N. Matsuzawa, A. Shimizu, T. Ota, M. Sakurai, H. Ando, K. Arai, T. Yamashita, M. Honda, T. Yamashita, S. Kaneko, Genes involved in oxidative phosphorylation are coordinately upregulated with fasting hyperglycaemia in livers of patients with type 2 diabetes, Diabetologia 50 (2007) 268–277.
[22] Y. Takeshita, T. Takamura, H. Ando, E. Hamaguchi, A. Takazakura, N. Matsuzawa-Nagata, S. Kaneko, Cross talk of tumor necrosis factor-alpha and the renin-angiotensin system in tumor necrosis factor-alpha-induced plasminogen activator inhibitor-1 production from hepatocytes, Eur. J. Pharmacol. 579 (2008) 426–432.
[23] T. Takamura, H. Misu, N. Matsuzawa-Nagata, M. Sakurai, T. Ota, A. Shimizu, S. Kurita, Y. Takeshita, H. Ando, M. Honda, S. Kaneko, Obesity upregulates genes involved in oxidative phosphorylation in livers of diabetic patients, Obesity, in press (Epub ahead of print).
[24] T. Takamura, H. Misu, T. Yamashita, S. Kaneko, SAGE application in the study of diabetes, Curr. Pharm. Biotechnol. 9 (2008) 392–399.
[25] A. Shimizu, T. Takamura, N. Matsuzawa, S. Nakamura, S. Nabemoto, Y. Takeshita, H. Misu, S. Kurita, M. Sakurai, M. Yokoyama, Y. Zen, M. Sasaki, Y. Nakanuma, S. Kaneko, Regulation of adiponectin receptor expression in human liver and a hepatocyte cell line, Metabolism 56 (2007) 1478–1485.
[26] H. Ando, Y. Oshima, H. Yanagihara, Y. Hayashi, T. Takamura, S. Kaneko, A. Fujimura, Profile of rhythmic gene expression in the livers of obese diabetic KK-A(y) mice, Biochem. Biophys. Res. Commun. 346 (2006) 1297–1302.
[27] N. Matsuzawa-Nagata, T. Takamura, H. Ando, S. Nakamura, S. Kurita, H. Misu, T. Ota, M. Yokoyama, M. Honda, K. Miyamoto, S. Kaneko, Increased oxidative stress precedes the onset of high-fat diet-induced insulin resistance and obesity, Metabolism 57 (2008) 1071–1077.
[28] M. Uno, S. Kurita, H. Misu, H. Ando, T. Ota, N. Matsuzawa-Nagata, Y. Kita, S. Nabemoto, H. Akahori, Y. Zen, Y. Nakanuma, S. Kaneko, T. Takamura, Tranilast, an antifibrogenic agent, ameliorates a dietary rat model of nonalcoholic steatohepatitis, Hepatology 48 (2008) 109–118.
[29] S. Kurita, T. Takamura, T. Ota, N. Matsuzawa-Nagata, Y. Kita, M. Uno, S. Nabemoto, K. Ishikura, H. Misu, H. Ando, Y. Zen, Y. Nakanuma, S. Kaneko, Olmesartan ameliorates a dietary rat model of non-alcoholic steatohepatitis through its pleiotropic effects, Eur. J. Pharmacol. 588 (2008) 316–324.
[30] R. Hardeland, A. Coto-Montes, B. Poeggeler, Circadian rhythms, oxidative stress, and antioxidative defense mechanisms, Chronobiol. Int. 20 (2003) 921–962.
[31] S. Langmesser, U. Albrecht, Life time-circadian clocks, mitochondria and metabolism, Chronobiol. Int. 23 (2006) 151–157.
[32] K. Obrietan, S. Impey, D.R. Storm, Light and circadian rhythmicity regulate MAP kinase activation in the suprachiasmatic nuclei, Nat. Neurosci. 1 (1998) 693–700.
[33] L. Fu, H. Pelicano, J. Liu, P. Huang, C. Lee, The circadian gene Period2 plays an important role in tumor suppression and DNA damage response in vivo, Cell 111 (2002) 41–50.
[34] T. Kudo, M. Akiyama, K. Kuriyama, M. Sudo, T. Moriya, S. Shibata, Night-time restricted feeding normalises clock genes and Pai-1 gene expression in the db/db mouse liver, Diabetologia 47 (2004) 1425–1436.
[35] L. Busino, F. Bassermann, A. Maiolica, C. Lee, P.M. Nolan, S.I. Godinho, G.F. Draetta, M. Pagano, SCFFbxl3 controls the oscillation of the circadian clock by directing the degradation of cryptochrome proteins, Science 316 (2007) 900–904.
[36] D. Gatfield, U. Schibler, Physiology. Proteasomes keep the circadian clock ticking, Science 316 (2007) 1135–1136.

Clinical and Experimental Hypertension, 31:201–207, 2009

ISSN: 1064-1963 print / 1525-6006 online
DOI: 10.1080/10641960902822450

informa
healthcare

Clock Gene Expression in the Liver and Adipose Tissues of Non-Obese Type 2 Diabetic Goto-Kakizaki Rats

HITOSHI ANDO,[1,2] KENTAROU USHIJIMA,[1]
HAYATO YANAGIHARA,[1] YOHEI HAYASHI,[1]
TOSHINARI TAKAMURA,[2] SHUICHI KANEKO,[2]
AND AKIO FUJIMURA[1]

[1]Division of Clinical Pharmacology, Department of Pharmacology, School of Medicine, Jichi Medical University, Tochigi, Japan
[2]Department of Disease Control and Homeostasis, Kanazawa University, Graduate School of Medical Science, Ishikawa, Japan

Recent studies have revealed a close relationship between the pathophysiology of metabolic syndrome, which is characterized by obesity and hyperglycemia, and the functioning of internal molecular clocks. In this study, we show that the rhythmic mRNA expression of clock genes (Clock, Bmal1, Cry1, and Dbp) is not attenuated in the liver and visceral adipose tissues of Goto-Kakizaki rats, a model of nonobese, type 2 diabetes, as compared to control Wistar rats. Our results suggest that molecular clock impairment in peripheral tissues of obese diabetic animals may be either caused by obesity-related factor(s), but not hyperglycemia, or be a cause, but not a consequence, of hyperglycemia.

Keywords circadian rhythm, clock gene, type 2 diabetes, metabolic syndrome, liver

Introduction

Various physiological and behavioral processes exhibit circadian (i.e., 24 h) rhythmicity, which in turn may play a pivotal role in maintaining functional homeostasis. Recent studies have revealed that these endogenous rhythms are generated at the cellular level by circadian core oscillators, composed of transcriptional/translational feedback loops involving a set of clock genes (1,2). In mammals, rhythmic transcriptional enhancement by two basic helix–loop–helix Per–Arnt–Sim domain-containing transcription factors, that is, CLOCK and brain and muscle Arnt-like protein 1 (BMAL1), provides the basic drive

Submitted August 20, 2007; revised December 19, 2007; accepted February 4, 2008.
Address correspondence to Akio Fujimura, MD, PhD, Department of Pharmacology, School of Medicine, Jichi Medical University, 3311-1 Yakushiji, Shimotsuke, Tochigi 329-0498, Japan; E-mail: akiofuji@jichi.ac.jp

for the intracellular clock system. Specifically, the CLOCK-BMAL1 heterodimer activates the transcription of various clock-controlled genes (3,4). Given that some clock-controlled genes, including the albumin D-site binding protein (Dbp), also serve as transcription factors, the expression of numerous genes may be tied to the functions of the molecular clock (1,2). In parallel, the heterodimer activates the transcription of several clock genes, including Period (Per) and Cryptochorome (Cry) (5–7). The resultant PER and CRY proteins translocate back into the nucleus and inhibit the activity of CLOCK-BMAL1, thus forming the negative feedback loop (1,2).

The molecular clock system resides not only in the hypothalamic suprachiasmatic nucleus (SCN), which is recognized as the central mammalian clock, but also in various peripheral tissues (8–11). The SCN is not essential for driving peripheral oscillations but acts to synchronize peripheral oscillators (10). Therefore, local molecular clocks may directly control the physiological rhythmicity of peripheral tissues.

Recently, type 2 diabetes mellitus has reached epidemic proportions (12). Pancreatic β-cell dysfunction and insulin resistance are key elements in the pathogenesis of type 2 diabetes and both contribute to the presence of hyperglycemia in this disease. In particular, insulin resistance is strongly associated with obesity, and several mechanisms mediating this interaction have been identified (12). For example, various humoral factors, so-called adipocytokines, which originate in adipose tissue, have been shown to modulate insulin action and may be involved in the development of various diseases including type 2 diabetes, hypertension, dyslipidemia, and cardiovascular disease (11,12). Interestingly, it has been demonstrated that clock mutant mice have an attenuated 24 h feeding rhythm, are hyperphagic and obese, and develop metabolic syndrome, including hyperglycemia and hyperlipidemia (13). In addition, BMAL1 and the clock gene Rev-erbα are known to be involved in the regulation of adipocyte differentiation (14,15). Impaired adipocyte differentiation, as well as increased adipocyte hypertrophy, plays major roles in the development of metabolic syndrome (16). Furthermore, previous studies have revealed that the rhythmic expression of clock genes is attenuated in the visceral adipose tissue and liver of genetically obese, diabetic mice (KK-A^y, ob/ob, and db/db mice) (11,17). Thus, a close relationship may exist between molecular clock functioning and the pathophysiology of obesity and/or type 2 diabetes. At this time, however, it remains to be elucidated whether type 2 diabetes, without obesity, is also associated with impaired molecular clock function. To address this issue, we investigated the rhythmic mRNA expression of clock genes in the visceral adipose tissue and liver of Goto-Kakizaki (GK) rats, a model of nonobese type 2 diabetes (18,19).

Materials and Methods

Rats

Eight-week-old male GK/Jcl and Wistar rats were obtained from CLEA Japan (Tokyo, Japan). All rats were maintained under specific pathogen-free conditions, controlled temperature, controlled humidity, and a 12-h light (07:00–19:00 h)/12-h dark (19:00–07:00 h) cycle. Rats were provided with a standard laboratory diet (CE-2, CLEA, Japan) and water *ad libitum*. After 2 weeks, animals were killed to obtain blood, liver, and epididymal fat samples at the following zeitgeber times (ZT): 0, 6, 12, and 18, where ZT 0 is defined as lights on and ZT 12 as lights off. All animal procedures were performed in accordance with the guidelines for animal research at Jichi Medical University, Japan.